



# The geographic mosaic of coevolution in mutualistic networks

Lucas P. Medeiros<sup>a,1</sup>, Guilherme Garcia<sup>a</sup>, John N. Thompson<sup>b</sup>, and Paulo R. Guimarães Jr.<sup>a,2</sup>

<sup>a</sup>Departamento de Ecologia, Instituto de Biociências, Universidade de São Paulo, 05508-090 São Paulo, SP, Brazil; and <sup>b</sup>Department of Ecology and Evolutionary Biology, University of California, Santa Cruz, CA 95064

Edited by May R. Berenbaum, University of Illinois at Urbana–Champaign, Urbana, IL, and approved October 11, 2018 (received for review May 28, 2018)

**Ecological interactions shape adaptations through coevolution not only between pairs of species but also through entire multispecies assemblages. Local coevolution can then be further altered through spatial processes that have been formally partitioned in the geographic mosaic theory of coevolution. A major current challenge is to understand the spatial patterns of coadaptation that emerge across ecosystems through the interplay between gene flow and selection in networks of interacting species. Here, we combine a coevolutionary model, network theory, and empirical information on species interactions to investigate how gene flow and geographical variation in selection affect trait patterns in mutualistic networks. We show that gene flow has the surprising effect of favoring trait matching, especially among generalist species in species-rich networks typical of pollination and seed dispersal interactions. Using an analytical approximation of our model, we demonstrate that gene flow promotes trait matching by making the adaptive landscapes of different species more similar to each other. We use this result to show that the progressive loss of gene flow associated with habitat fragmentation may undermine coadaptation in mutualisms. Our results therefore provide predictions of how spatial processes shape the evolution of species-rich interactions and how the widespread fragmentation of natural landscapes may modify the coevolutionary process.**

coadaptation | ecological networks | gene flow | mutualism | trait matching

**E**cological interactions are a fundamental component of biodiversity (1). Phenotypic traits of many species have evolved through selection imposed by ecological interactions, such as toxins in prey and resistance to toxins in their predators (2) or floral tubes of plants and mouthparts of their pollinators (3). These examples show how reciprocal selection shapes coadaptation in pairs or small groups of interacting species. However, small groups of species rarely interact in isolation. Species are usually embedded in networks containing dozens or even hundreds of interacting species (4, 5). Understanding how patterns of coadaptation arise and favor species persistence in large assemblages of interacting species is currently a major challenge requiring approaches at the interface of ecology, evolution, and network science (6–8).

For mutualisms, previous studies have explored how coevolution may affect network architecture—that is, the pattern of interactions among species—and, in turn, how such architecture may drive coevolution. The role of coevolution in shaping the organization of links of empirical networks is still uncertain (9–12). Nevertheless, it is known that network architecture varies with fundamental aspects of the natural history of interactions, potentially leading to distinct coevolutionary dynamics (7, 13). For example, multiple-partner mutualisms, in which an individual interacts with several individuals throughout its life, such as pollination or seed dispersal by animals, typically form species-rich and nested networks (14, 15). Theoretical evidence suggests that coevolution in multiple-partner mutualisms operates in part through indirect evolutionary effects—that is, evolutionary outcomes caused by species that are not

linked as interacting partners (7), favoring similarity in traits at the community level (i.e., trait convergence) (16, 17). In contrast, intimate mutualisms, in which an individual completes at least a life stage on a single host, such as protection of host plants by ants or protection of anemonefishes by host anemones, generate species-poor and modular networks (18, 19). Coevolution in intimate mutualisms is expected to exhibit frequent and reciprocal effects between species that interact directly (13), leading to the tight trait matching observed in many intimate interactions (20). Thus, studies of coevolution in mutualistic networks have shown how adaptive landscapes may be modified by the underlying network structure, molding trait patterns (Fig. 1A).

Coevolution in multispecific interactions, however, is a geographic process, as the assembly of interaction networks and the ongoing coevolution in these networks may vary across space (1). In pairs or small groups of species, theoretical and empirical work on the geographic mosaic of coevolution have shown that patterns of adaptation vary widely across geographic regions depending on the distribution of local selection regimes (2, 21–23). In addition, the connection of different populations via gene flow as well as other genetic and genomic processes may remix trait distributions across the landscape, promoting or inhibiting the evolution of local coadaptation (24–27). Although gene

## Significance

**The reciprocal evolution of interacting species, or coevolution, generates impressive adaptations in pairs of species across geographic regions. However, we currently do not understand how coevolution shapes adaptations in large groups of species that interact not just locally but also across ecosystems. We use a mathematical model of coevolution and network tools to show that gene flow resulting from movement of individuals among populations may favor, rather than swamp, reciprocal adaptation in mutualisms, especially in large and heterogeneous networks typical of pollination and seed dispersal interactions. Our results suggest that the disruption of gene flow, fueled by human activities, may undermine long-term adaptation in mutualistic assemblages, with severe consequences for the functioning of ecological systems.**

Author contributions: L.P.M., J.N.T., and P.R.G. designed research; L.P.M. performed numerical simulations; L.P.M. and G.G. obtained analytical results; L.P.M. and G.G. analyzed data; and L.P.M., J.N.T., and P.R.G. wrote the paper.

The authors declare no conflict of interest.

This article is a PNAS Direct Submission.

Published under the [PNAS license](#).

Data deposition: All of the codes and empirical datasets required to reproduce our results are available at [https://github.com/wgar84/spatial\\_coevo\\_mutnet](https://github.com/wgar84/spatial_coevo_mutnet).

<sup>1</sup>Present address: Department of Civil and Environmental Engineering, MIT, Cambridge, MA 02139.

<sup>2</sup>To whom correspondence should be addressed. Email: prguima@usp.br.

This article contains supporting information online at [www.pnas.org/lookup/suppl/doi:10.1073/pnas.1809088115/-DCSupplemental](http://www.pnas.org/lookup/suppl/doi:10.1073/pnas.1809088115/-DCSupplemental).

Published online November 7, 2018.

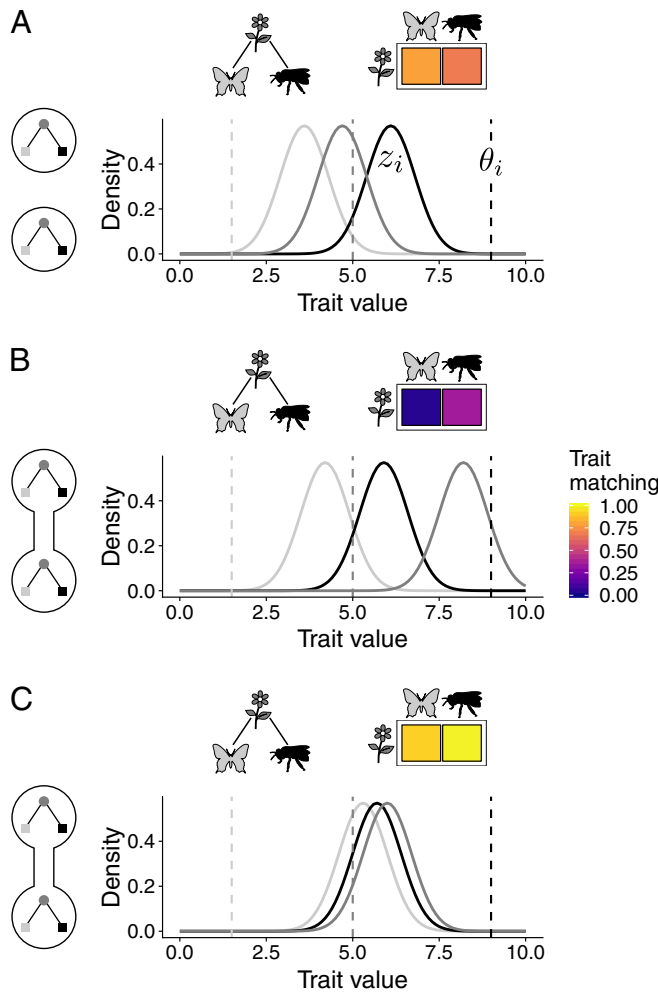


**Fig. 1.** Potential effects of gene flow on trait evolution in mutualistic networks. In this example, there are two sites in which the same two pollinator species interact with the same plant species. Each curve represents a trait distribution with mean  $z_i$  of one population in one of the sites (light gray and black: pollinator species; dark gray: plant species). Dashed lines indicate the trait values favored by the local environment ( $\theta_i$ ). (A) In the absence of gene flow across sites, trait matching (colors in the interaction matrix) evolves because mutualistic interactions modify local adaptive landscapes. (B and C) Gene flow across sites with distinct selection regimes may shift species traits, further altering adaptive landscapes and trait patterns in two possible ways. (B) First, gene flow may induce trait mismatching. (C) Second, gene flow may strengthen the coadaptation pattern previously observed for the isolated assemblage.

flow may strengthen local adaptation by increasing the genetic variation available to selection in some systems (28), this mechanism alone is unlikely in coevolving systems, in which gains in genetic variation would not compensate the deviations from local adaptation (21).

Despite the importance of gene flow and geographical variation in selection in interactions involving few species, we currently lack a framework to understand how these processes shape trait evolution in species-rich metacommunities (29, 30). In spatial metanetworks (31), the interplay between gene flow, geographical variation in selection, and both direct and indirect coevolutionary effects may reshape local adaptive landscapes with important consequences for trait evolution (Fig. 1B and C).

Here, we combine a mathematical model of coevolution, network theory, and empirical data on species interactions to

develop a framework that merges the geographic mosaic of coevolution with coevolutionary networks. We use this framework to investigate how the interplay between gene flow, geographical variation in selection, and network structure may affect the emergence of coadaptation in mutualisms. Through numerical simulations parameterized by 72 empirical networks, we show that gene flow increases trait matching between mutualistic partners, especially in species-rich, nested networks. Additional simulations using an analytical approximation of our model show that the progressive loss of gene flow due to habitat fragmentation could undermine coadaptations by altering species adaptive landscapes.

## Results

**Gene Flow, Geographical Variation in Selection, and the Evolution of Trait Patterns.** We first explored the emergence of trait matching in a single site using a previously developed model (7) that describes the evolution of a single trait shaped by mutualistic interactions among populations of different species (*Materials and Methods*). In this model, the mean trait value of each species ( $z_i$ ) evolves toward a fixed environmental optimum ( $\theta_i$ ) in the absence of mutualism. Mutualistic selection modifies this simple adaptive landscape by favoring trait matching among mutualistic partners (Fig. 1A). We performed numerical simulations of this model parameterized by the structure of 72 empirical mutualistic networks (*SI Appendix, Table S1*). We found that increasing mutualistic selection ( $m_i$ ) leads to stronger reciprocal selection and to higher trait matching (*SI Appendix, Fig. S1*). As a consequence, networks in which  $m_i$  is high and there is strong reciprocal selection (hereafter hotspots) favor higher levels of trait matching than networks in which  $m_i$  is low and there is weak reciprocal selection (hereafter coldspots).

We next extended the coevolutionary model to two sites to explore how gene flow and geographical variation in mutualistic selection affect trait evolution (*Materials and Methods*). We performed simulations parameterized by our 72 empirical networks, assuming that the same network occurs at both sites. We found that gene flow ( $g_i$ ) can either enhance or reduce trait matching, depending on mutualistic selection. For the majority of combinations of mutualistic selection, including two hotspots ( $\bar{m}_A = \bar{m}_B = 0.7$ ), gene flow favors the emergence of trait matching (Fig. 2A and *SI Appendix, Fig. S2*). This surprising effect occurs because gene flow cancels out local conflicting selective pressures and allows trait matching to evolve, especially in pairs of generalist species (i.e., species with many interactions; Fig. 2A and *SI Appendix, Fig. S3*). This effect of gene flow results both from the uncoupling of species traits from their environmental optima and from the geographical homogenization of traits (*SI Appendix, Fig. S4*).

Importantly, gene flow promotes trait matching especially when environmental optima ( $\theta_{i,A}, \theta_{i,B}$ ) are not correlated across sites, meaning that the selection regime of each species varies geographically as a selection mosaic (*SI Appendix, Fig. S5*). For a few combinations of mutualistic selection, such as a hotspot and a coldspot ( $\bar{m}_A = 0.9, \bar{m}_B = 0.1$ ), gene flow disrupts trait matching at the hotspot (Fig. 2B and *SI Appendix, Fig. S2*). In this case, populations at the coldspot are trapped into their environmental optima, and gene flow inhibits the evolution of trait matching at the hotspot. Sensitivity analyses showed that these results hold for many different parameter values (*SI Appendix, Table S2* and *Fig. S5*), for a scenario in which gene flow is greater in generalist than in specialist species (*SI Appendix, Fig. S6*), and for a scenario in which species composition and network structure vary across sites (*SI Appendix, Fig. S7*).

We then obtained analytical equilibrium expressions to understand how coevolution shapes trait patterns (*SI Appendix*). With a single site, the trait values at equilibrium (vector  $\mathbf{z}^*$ ) are connected to species environmental optima (vector  $\boldsymbol{\theta}$ ) through

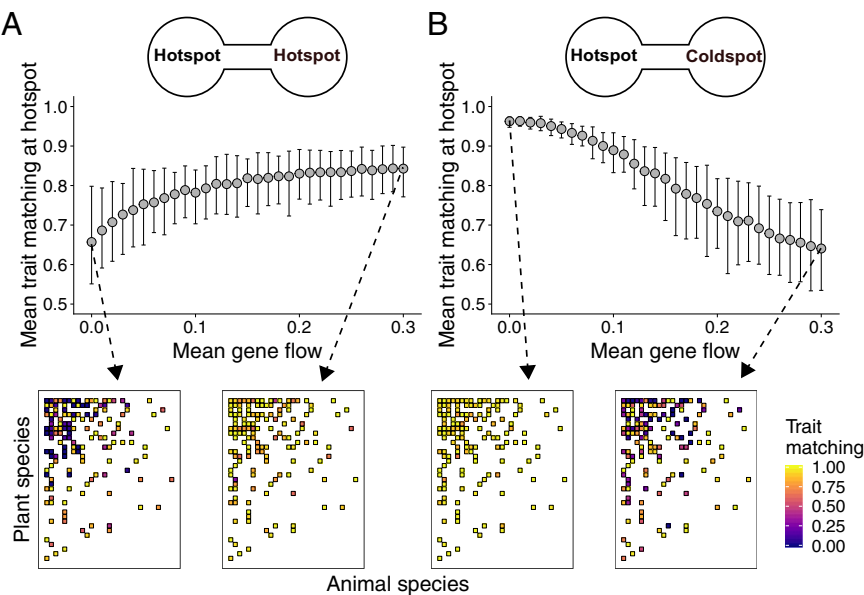


**Fig. 2.** Effects of gene flow on the evolution of trait matching in mutualistic networks. (A and B) Each point is the mean trait matching at equilibrium at the hotspot ( $\bar{\tau}_A^*$ ) for 100 simulations parameterized with a seed dispersal network (network 64 in *SI Appendix*, Table S1), and bars show the 95% confidence interval. (A) When mutualistic selection is high at both sites ( $\bar{m}_A = \bar{m}_B = 0.7$ ), gene flow favors trait matching at each hotspot. (B) When mutualistic selection is high at only one site ( $\bar{m}_A = 0.9$ ,  $\bar{m}_B = 0.1$ ), gene flow reduces trait matching at the hotspot. Changes in mean trait matching (A and B) are a consequence of changes in the matching among generalist species, as shown in the interaction matrices (colors depict equilibrium pairwise trait matching for one simulation with the indicated value of gene flow). Sample distributions and values for simulation parameters:  $\varphi_{i,A}, \varphi_{i,B} \sim \mathcal{N}[\mu = 0.5, \sigma^2 = 10^{-4}]$ ,  $\theta_{i,A} \sim \mathcal{U}[0, 10]$ ,  $\theta_{i,B} \sim \mathcal{U}[10, 20]$ ,  $m_{i,A} \sim \mathcal{N}[\bar{m}_A, 10^{-4}]$ ,  $m_{i,B} \sim \mathcal{N}[\bar{m}_B, 10^{-4}]$ ,  $g_i \sim \mathcal{N}[\bar{g}, 10^{-6}]$ , and  $\alpha = 0.2$ .

a matrix ( $\mathbf{T}$ ) that contains direct and indirect coevolutionary effects:  $\mathbf{z}^* = \mathbf{T}\boldsymbol{\theta}$  (7). Row  $i$  of  $\mathbf{T}$  represents how other species directly or indirectly affect the adaptive landscape of species  $i$ . By measuring the correlation among rows of  $\mathbf{T}$ , we showed that similar mutualistic adaptive landscapes among species favor trait matching and trait convergence (*SI Appendix*). Moreover, we found that increasing mutualistic selection leads to greater similarity of adaptive landscapes and higher trait matching, because indirect effects become stronger when mutualistic selection is higher (*SI Appendix*, Figs. S8 and S9). With two sites, the matrix  $\mathbf{T}$  combines direct and indirect coevolutionary effects within and between sites. We found that increasing gene flow contributes to the similarity of adaptive landscapes, fueling trait matching in both mutualistic assemblages (*SI Appendix*, Figs. S10 and S11A). It does so by expanding the indirect effects of mutualistic selection across sites. In contrast, gene flow between a hotspot and a coldspot has an opposite effect and decreases trait matching (*SI Appendix*, Fig. S11B).

**Network Structure and the Evolution of Trait Patterns.** Our next step was to investigate how network structure influences coevolution and mediates the effects of gene flow. We characterized the structure of our 72 empirical networks using four metrics: species richness, connectance, nestedness, and modularity (*Materials and Methods*). We performed a Principal Component Analysis (PCA) of these metrics to obtain two variables ( $PC_1$  and  $PC_2$ ) that describe the range of variation in network structure in our empirical dataset (Fig. 3A and *SI Appendix*, Table S1).

In the absence of gene flow, species-poor, modular networks typical of intimate mutualisms favored the evolution of higher levels of trait matching than species-rich, nested networks typical of multiple-partner mutualisms (Fig. 3B, multiple linear regression:  $\bar{\tau}^* \sim 0.73 - 0.01PC_1 - 0.05PC_2$ ,  $\bar{m} = 0.7$ ,  $\bar{g} = 0$ ). When gene flow is present, however, network structure has a weaker effect on the emergence of trait matching, allowing multiple-partner mutualisms to attain levels of trait

matching almost as high as the ones observed for intimate mutualisms (Fig. 3C,  $\bar{\tau}_A^* \sim 0.86 - 0.005PC_1 - 0.01PC_2$ ,  $\bar{m}_A = \bar{m}_B = 0.7$ ,  $\bar{g} = 0.3$ ). This result occurs because networks of multiple-partner mutualisms contain a core of interacting generalists and the effect of gene flow on trait matching is stronger for pairs of generalist species than for other pairs of species (*SI Appendix*, Fig. S3). Our simulations using other combinations of mutualistic selection ( $\bar{m}_A, \bar{m}_B$ ) support the interpretation that gene flow has a stronger effect on multiple-partner mutualisms (*SI Appendix*, Fig. S2).

**Disruption of Gene Flow and Its Consequences for Coevolution.** Having shown that gene flow may favor the emergence of coadaptation in mutualistic networks, we next considered the consequences of the disruption of gene flow to trait evolution. To do so, we simulated a progressive loss of gene flow in two initially connected mutualistic assemblages and computed equilibrium trait values using our analytical approximation (*Materials and Methods*). We used empirical information on ecological dependencies between mutualistic partners (i.e., weights in adjacency matrices; *SI Appendix*, Table S1) of 29 networks in our dataset to parameterize the evolutionary effects ( $q_{ij}$ ) of the matrix  $\mathbf{T}$ . By removing gene flow from an increasing fraction of species, we altered the direct and indirect coevolutionary effects within and between networks present in  $\mathbf{T}$ .

We found that the ongoing disruption of gene flow causes trait matching to decrease, but extreme loss of gene flow may recover some level of trait matching (Fig. 4 and *SI Appendix*, Fig. S12). Further analysis revealed that the lowest values of trait matching in these simulations occur when gene flow is highly variable across species in the network (*SI Appendix*, Fig. S13).

## Discussion

The geographical and multispecific complexity of coevolution poses a challenge to our understanding of the evolution of

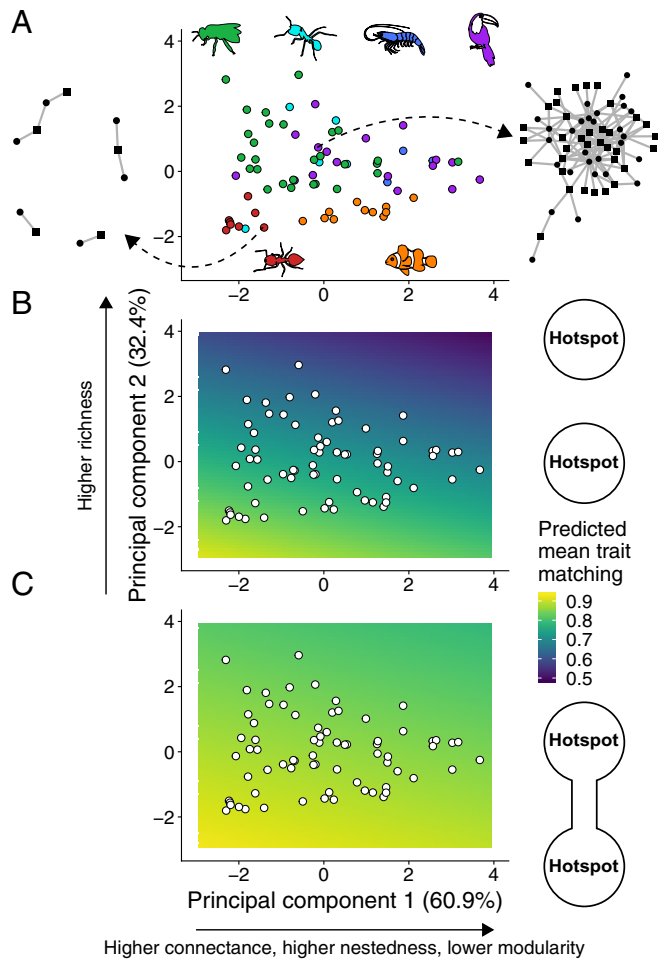


**Fig. 3.** Network structure, gene flow, and the emergence of trait matching in mutualistic networks. (A) PC1 and PC2 of a PCA using four network structure metrics measured for our 72 empirical networks. PC1 accounted for 60.9% of all variation and was strongly correlated with connectance (0.56), nestedness (0.58), and modularity ( $-0.56$ ). PC2 accounted for 32.4% of all variation and was strongly correlated with species richness (0.81). Network structure was highly variable, as illustrated by an ants-myrmecophytes (Left, network 14 in *SI Appendix*, Table S1) and a seed dispersal (Right, network 64 in *SI Appendix*, Table S1) network. Types of mutualism: green, pollination; cyan, ants–nectary-bearing plants; dark blue, marine cleaning; purple, seed dispersal; red, ants–myrmecophytes; orange, anemones–anemonefishes. (B and C) Predicted mean trait matching at the hotspot ( $\bar{\tau}_A^*$ ) for a linear model with PC1 and PC2 as explanatory variables and trait matching from simulations as the response variable (white points are the networks in A). (B) Species-poor, modular networks favored the emergence of trait matching in isolated hotspots ( $\bar{m} = 0.7$ ,  $\bar{g} = 0$ ,  $n = 100$  simulations per network). (C) The effect of network structure is reduced when the two hotspots are connected by gene flow, and species-rich, nested networks may also favor high trait matching ( $\bar{m}_A = \bar{m}_B = 0.7$ ,  $\bar{g} = 0.3$ ,  $n = 100$  simulations per network). Simulation parameters as in Fig. 2.

interacting species. In this study, we tackled this challenge by taking a first step in merging the geographic mosaic theory of coevolution with the recent approach of coevolutionary networks. Our framework combines a coevolutionary model and network theory to evaluate how gene flow, hotspots, and coldspots shape trait matching in multiple-partner and intimate mutualisms. Our findings reveal three main ways in which gene flow may be a fundamental process catalyzing the evolution of coadaptation in species-rich systems across simple landscapes.

First, gene flow may promote trait matching among mutualists within large networks. Previous results have shown that gene flow is capable of promoting adaptive evolution in natural populations by increasing local genetic variation (28) or when individuals disperse to specific habitats (32). Here, we reveal an additional mechanism for how gene flow may contribute to adaptation. When two mutualistic assemblages are connected by gene flow, the effects of environmental selection are canceled out, allowing mutualistic selection to drive trait evolution. As a consequence, gene flow makes the adaptive landscape of different species more similar to each other, erasing the conflicting selective pressures on highly interacting species and allowing trait matching and trait convergence to emerge. This result may provide a mechanism for one of the most challenging problems in coevolution, which is how local adaptation scales up to generate trait patterns in interacting species across broad geographical areas. We also found that gene flow may reduce trait matching for some specific scenarios, such as when a hotspot is linked to a coldspot. Therefore, specific combinations of gene flow and geographical variation in selection may generate trait mismatching in interacting species (2, 21). By analyzing pairs of interacting species, we showed that the observed changes in coadaptation patterns are mainly driven by species with a high number of interactions, such as generalist bees in pollination networks (33). This result, combined with our simulations incorporating simple spatial turnover in species composition, allows us to hypothesize that the observed effects of gene flow and geographical variation in selection should hold whenever generalist species are consistently present across local interaction networks. Our conclusions, however, may not hold for more complex landscapes, in which spatial heterogeneity may lead to unanticipated evolutionary dynamics.

Second, we show that network architecture mediates the effects of gene flow and geographical variation in selection on the evolution of trait patterns. The study of coadaptation in mutualistic

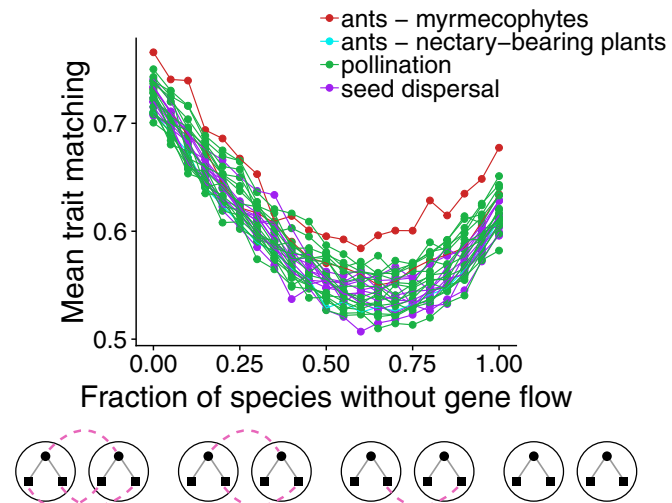


**Fig. 4.** Disruption of gene flow and its consequences for trait matching in mutualistic networks. Trait matching decreases as gene flow is progressively lost in mutualistic networks but increases slightly with an extreme loss of gene flow. Initially, all species in the network have a high value of gene flow ( $g_i = 0.3 \forall i$ ), and species randomly lose gene flow until all species lack gene flow ( $g_i = 0 \forall i$ ). Each point is the mean equilibrium trait matching at site A ( $\bar{\tau}_A^*$ ) calculated with our analytical equilibrium expression using 10 different environmental optimum ( $\theta$ ) samples in each of 10 distinct simulations. Lines connect points from the same network, and different colors indicate different types of mutualism. Sample distributions and values for simulation parameters:  $\varphi_{i,A} = \varphi_{i,B} = 1$ ,  $\theta_{i,A} \sim \mathcal{U}[0, 10]$ ,  $\theta_{i,B} \sim \mathcal{U}[10, 20]$ ,  $m_{i,A} = m_{i,B} = 0.5$ , and  $\alpha = 0.2$ .

systems has often focused on specialized interactions, such as the protection of host plants by their sheltered ant colonies (20, 34). In small networks of specialized species, coevolution should operate through frequent reciprocal changes between interacting species, generating impressive matching between morphological or physiological traits (20, 23, 34). However, in networks with dozens of interacting partners, coevolution may proceed through indirect effects (7), potentially driving community-level trait patterns such as trait convergence in assemblages of mimetic species (35) or fruiting plants (16). Because our results indicate that gene flow favors coadaptation mainly among generalist species, the effect of gene flow is greater in species-rich, nested networks than in species-poor, modular networks. Thus, networks of intimate mutualisms such as protective ants and their host myrmecophytes may favor tight trait matching between interacting partners irrespective of how well-connected populations are across a landscape. In contrast, the emergence of strong trait matching in multiple-partner mutualisms such as pollination may be contingent upon gene flow between populations.

Third, the trait patterns observed in species-rich mutualisms may be fragile in the face of processes leading to the disruption of gene flow, such as habitat fragmentation. Habitat fragmentation is one of the most widespread environmental impacts of human activities (36). Because habitat fragmentation may disrupt gene flow, genetic variability may wane in isolated populations, with severe consequences for the persistence of such populations (37). Our results suggest an additional effect of the gradual disruption of gene flow: the loss of coadaptation in mutualistic systems. This loss of coadaptation could, in turn, erode the potential robustness of coevolved interaction networks to human disturbance (8). We hypothesize, therefore, that habitat fragmentation may cause species-rich mutualisms to lose their ecological effects over time, with severe consequences for ecosystem services such as crop pollination and regeneration of plant populations (38).

## Materials and Methods

**Single-Site Coevolutionary Model.** We first used a single-site coevolutionary model to explore the emergence of trait patterns (7) (*SI Appendix*). This model is based on a selection gradient that connects trait evolution with the mean fitness consequences of mutualisms. In this model,  $N$  populations of distinct species interact mutualistically at a given site, and the mean value of a single trait of each population ( $z_i$ ) evolves in discrete time. Trait  $z_i$  mediates mutualistic interactions (e.g., flower tube length, pollinator mouthpart length) and affects the fitness consequences of the mutualism (mutualistic selection) as well as other fitness components, such as abiotic factors (environmental selection). The trait evolution of species  $i$  is described as follows:

$$z_i^{(t+1)} = z_i^{(t)} + \varphi_i \left[ \sum_{j=1}^N q_{ij}^{(t)} (z_j^{(t)} - z_i^{(t)}) + \left( 1 - \sum_{j=1}^N q_{ij}^{(t)} \right) (\theta_i - z_i^{(t)}) \right], \quad [1]$$

where  $\varphi_i$  is proportional to the slope of the selection gradient and to the additive genetic variance of the trait,  $q_{ij}^{(t)}$  represents the evolutionary effect of species  $j$  on species  $i$  ( $0 \leq q_{ij}^{(t)} \leq 1$ ), and  $\theta_i$  is the trait value favored by the environment. We assumed that mutualistic selection is mediated by trait matching and, therefore, the trait value of species  $i$  favored by selection imposed by species  $j$  is  $z_j$ . The evolutionary effects  $q_{ij}^{(t)}$  are defined as a function of trait matching as:

$$q_{ij}^{(t)} = m_i \frac{a_{ij} \tau_{ij}^{(t)}}{\sum_{k=1}^N a_{ik} \tau_{ik}^{(t)}}, \quad [2]$$

where  $m_i$  measures the relative importance of all mutualistic interactions ( $0 \leq \sum_{j=1}^N q_{ij}^{(t)} = m_i \leq 1$ ),  $a_{ij}$  is an element of  $\mathbf{A}$ —the binary adjacency matrix of a given mutualistic network—and  $\tau_{ij}^{(t)}$  is the level of trait matching between  $i$  and  $j$  ( $0 \leq \tau_{ij}^{(t)} \leq 1$ ). We defined trait matching as  $\tau_{ij}^{(t)} =$

$e^{-\alpha(z_j^{(t)} - z_i^{(t)})^2}$ , in which  $\alpha$  controls the sensitivity of  $\tau_{ij}^{(t)}$  to differences between traits. If species  $i$  and  $j$  do not interact in the mutualistic network, then  $a_{ij} = 0$  and  $q_{ij}^{(t)}$  is an evolutionary forbidden link. In contrast, if  $i$  and  $j$  are mutualistic partners, then  $a_{ij} = 1$  and  $q_{ij}^{(t)}$  changes through time according to trait matching.

**Two-Site Coevolutionary Model.** We extended the single-site coevolutionary model to a scenario with two mutualistic assemblages connected by gene flow (*SI Appendix*), which is consistent with the concept of a spatial metanetwork (31). We assumed that, at each generation, a fraction  $g_i$  of the individuals of species  $i$  migrate from site  $A$  to site  $B$  and from site  $B$  to site  $A$  ( $0 \leq g_i \leq 1$ ). Thus, a fraction  $1 - g_i$  of all individuals in both populations remains at its own site. The mean trait value of species  $i$  at site  $A$  changes according to the following equation:

$$z_{i,A}^{(t+1)} = (1 - g_i) (z_{i,A}^{(t)} + \delta_{z_{i,A}}^{(t)}) + g_i (z_{i,B}^{(t)} + \delta_{z_{i,B}}^{(t)}), \quad [3]$$

where  $\delta_{z_{i,A}}^{(t)} = \varphi_{i,A} \left[ \sum_{j=1}^{N_A} q_{ij,A}^{(t)} (z_{j,A}^{(t)} - z_{i,A}^{(t)}) + \left( 1 - \sum_{j=1}^{N_A} q_{ij,A}^{(t)} \right) (\theta_{i,A} - z_{i,A}^{(t)}) \right]$ . The term  $\delta_{z_{i,B}}^{(t)}$  and the equation for the evolutionary change in  $z_{i,B}$  are obtained by interchanging subscripts  $A$  and  $B$  in  $\delta_{z_{i,A}}^{(t)}$  and in Eq. 3. Importantly, model parameters ( $\varphi_i$ ,  $m_i$ ,  $\theta_i$ ), species richness ( $N$ ), and interaction networks ( $a_{ij}$ ) can all vary across sites, which allowed us to explore how geographical variation in these components affects trait evolution (*SI Appendix*).

**Simulations of the Coevolutionary Models.** We performed numerical simulations of the coevolutionary models to investigate how mutualistic selection ( $m_{i,A}$ ,  $m_{i,B}$ ) and gene flow ( $g_i$ ) influence the emergence of trait matching ( $\tau_{ij}^{(t)}$ ) (*SI Appendix*). First, we explored how mutualistic selection affects reciprocal selection and trait matching in an isolated site by performing simulations of the single-site model (Eq. 1), using different values of the mean mutualistic selection in the network ( $\bar{m} = 0.1, 0.3, 0.5, 0.7, 0.9$ ). Then, we focused on how the mean value of gene flow in the network ( $\bar{g}$ ), which we varied from 0 to 0.3, affects the evolution of trait matching in two connected hotspots ( $\bar{m}_A = \bar{m}_B = 0.7$ ) in which reciprocal selection among species was strong and in a hotspot connected to a coldspot ( $\bar{m}_A = 0.9$ ,  $\bar{m}_B = 0.1$ ) in which reciprocal selection was weak. For each combination of  $\bar{m}_A$ ,  $\bar{m}_B$ , and  $\bar{g}$ , we performed 100 simulations of the two-site model (Eq. 3) per empirical mutualistic network in our dataset ( $n = 72$  networks, *SI Appendix*, Table S1). In all simulations with the same empirical network, we parameterized the term  $a_{ij}$  by setting  $a_{ij} = 1$  when species  $i$  and  $j$  interacted in the network and  $a_{ij} = 0$  otherwise. All other parameters ( $\varphi_{i,A}$ ,  $\varphi_{i,B}$ ,  $\theta_{i,A}$ ,  $\theta_{i,B}$ ,  $\alpha$ ) and initial trait values ( $z_{i,A}^{(0)}$ ,  $z_{i,B}^{(0)}$ ) were sampled at the beginning of each simulation from statistical distributions (*SI Appendix*, Table S2). In each simulation, we recorded trait values through time and computed trait matching for pairs of species ( $\tau_{ij}^{(t)}$ ) as well as the mean value across all interacting species ( $\bar{\tau}^{(t)}$ ) at both sites. The equilibrium values of trait matching ( $\bar{\tau}_A^*$  and  $\bar{\tau}_B^*$ ) were calculated when species traits at both sites achieved asymptotic values, defined as  $|z_{i,A}^{(t+1)} - z_{i,A}^{(t)}| < 10^{-6}$  and  $|z_{i,B}^{(t+1)} - z_{i,B}^{(t)}| < 10^{-6}$ . In addition to performing simulations, we obtained analytical approximations of the coevolutionary models (Eqs. 1 and 3) to understand how trait patterns emerge in mutualistic networks (*SI Appendix*). All of the codes and empirical datasets required to reproduce our results are available at [https://github.com/wgar84/spatial\\_coevo\\_mutnet](https://github.com/wgar84/spatial_coevo_mutnet).

**Empirical Dataset.** Our dataset consisted of 72 empirical networks of both terrestrial and marine mutualisms (*SI Appendix*, Table S1). We chose these networks because they spanned diverse natural history attributes and network structures. Our dataset included six types of mutualism that can be divided into two broad categories: first, multiple-partner mutualisms in which individuals may interact with dozens or hundreds of different partners over a lifetime and form species-rich, nested networks—(i) ants that protect plants with extrafloral nectaries ( $n = 5$  networks), (ii) animals that pollinate flowering plants ( $n = 28$ ), (iii) fruit-eating vertebrates that disperse the seeds of plants with fleshy fruits ( $n = 17$ ), and (iv) fishes and shrimps that clean client fishes ( $n = 3$ ); second, intimate mutualisms in which individuals create sustained interactions and form species-poor, modular networks: (v) anemones that protect anemonefishes ( $n = 11$ ) and (vi) ants that protect their host plants, the myrmecophytes ( $n = 8$ ).

**Network Structure.** We quantified four widely used metrics to characterize the arrangement of interactions in our networks: (i) species richness, (ii) connectance, (iii) nestedness, and (iv) modularity (*SI Appendix*). We used only information on the presence and absence of interactions (i.e., 1 and 0) to quantify these metrics. Species richness ( $N$ ) is the total number of species in the network. Connectance ( $C$ ) is the proportion of all possible interactions that are in fact realized (14). Nestedness measures how much the interactions of species with low degree values are proper subsets of the interactions of species with higher degree values (15). We quantified nestedness using the metric *NODF* (39). Finally, modularity measures how much the network is partitioned into groups of species with many interactions within groups and few interactions among different groups (33). We computed modularity using a simulated annealing algorithm to optimize the value of a bipartite version of the metric  $Q$  (40). Because network structure metrics are often highly correlated among each other, we used PCA to describe how the values of our four metrics covary across networks. We used the first and second principal components ( $PC_1$  and  $PC_2$ ) to describe the variation in network structure of our dataset and to explore how network structure affects the emergence of trait patterns.

**Disruption of Gene Flow and Its Consequences for Coevolution.** We used our analytical approximation of the coevolutionary model to simulate the

progressive loss of gene flow in two initially connected mutualistic assemblages (*SI Appendix*). We began each simulation by building a matrix  $T$  with  $m_{i,A} = m_{i,B} = 0.5 \forall i$  and a high value of gene flow ( $g_i = 0.3 \forall i$ ). We used the ecological dependencies between interacting species (i.e., weights in adjacency matrices; *SI Appendix, Table S1*) available for 29 networks in our dataset as proxies for the evolutionary effects ( $q_{ij}$ ) in  $T$ . Then, we perturbed  $T$  by randomly removing gene flow from an increasing proportion of species (i.e., 0.05, 0.1, ..., 0.95, 1 of species without gene flow). The simulation ended when all species had lost gene flow ( $g_i = 0 \forall i$ ). After each perturbation of matrix  $T$ , we sampled 10 different  $\theta$  vectors using a statistical distribution and used our analytical equilibrium expression to calculate trait values ( $z^*$ ) and trait matching ( $\gamma_j^*$ ). We performed simulations for many different combinations of  $m_{i,A}$ ,  $m_{i,B}$ , and  $g_i$  (*SI Appendix*).

**ACKNOWLEDGMENTS.** We thank P. I. Prado, R. Vicente, R. Cogni, G. Marroig, C. Reigada, P. Jordano, M. M. Pires, F. M. D. Marquitti, M. Galetti, and members of the P.R.G. laboratory for suggestions and discussions regarding this work. We also thank the researchers that kindly provided their empirical datasets. Icons are under public domain except for flower (Ab-dul Wahhab), anemonefish (parkjisun), toucan (Sma-rtez), and shrimp (Jerey Qua). L.P.M. was supported by Fundação de Amparo à Pesquisa do Estado de São Paulo (FAPESP) Grant 2015/12956-7. P.R.G. was supported by FAPESP Grants 2016/20739-9 and 2017/08406-7 and Conselho Nacional de Desenvolvimento Científico e Tecnológico.

1. Thompson JN (2005) *The Geographic Mosaic of Coevolution* (Univ of Chicago Press, Chicago).
2. Hanifin CT, Brodie ED, Brodie ED (2008) Phenotypic mismatches reveal escape from arms-race coevolution. *PLoS Biol* 6:0471–0482.
3. Pauw A, Stofberg J, Waterman RJ (2009) Flies and flowers in Darwin's race. *Evolution* 63:268–279.
4. McCann KS (2011) *Food Webs* (Princeton Univ Press, Princeton).
5. Bascompte J, Jordano P (2014) *Mutualistic Networks*. (Princeton Univ Press, Princeton).
6. Andreazzi CS, Thompson JN, Guimarães PR, Jr. (2017) Network structure and selection asymmetry drive coevolution in species-rich antagonistic interactions. *Am Nat* 190:99–115.
7. Guimarães PR, Pires MM, Jordano P, Bascompte J, Thompson JN (2017) Indirect effects drive coevolution in mutualistic networks. *Nature* 550:511–514.
8. Nuismer SL, Week B, Aizen MA (2018) Coevolution slows the disassembly of mutualistic networks. *Am Nat* 192:490–502.
9. Nuismer SL, Jordano P, Bascompte J (2013) Coevolution and the architecture of mutualistic networks. *Evolution* 67:338–354.
10. Hui C, Minoarvelo HO, Landi P (2017) Modelling coevolution in ecological networks with adaptive dynamics. *Math Meth Appl Sci*, in press.
11. Ponisio LC, M'Gonigle LK (2017) Coevolution leaves a weak signal on ecological networks. *Ecosphere* 8:e01798.
12. Valverde S, et al. (2018) The architecture of mutualistic networks as an evolutionary spandrel. *Nat Ecol Evol* 2:94–99.
13. Guimarães PR, et al. (2007) Interaction intimacy affects structure and coevolutionary dynamics in mutualistic networks. *Curr Biol* 17:1797–1803.
14. Jordano P (1987) Patterns of mutualistic interactions in pollination and seed dispersal: Connectance, dependence asymmetries, and coevolution. *Am Nat* 129:657–677.
15. Bascompte J, Jordano P, Melián CJ, Olesen JM (2003) The nested assembly of plant-animal mutualistic networks. *Proc Natl Acad Sci USA* 100:9383–9387.
16. Lomascolo SB, Levey DJ, Kimball RT, Bolker BM, Alborn HT (2010) Dispersers shape fruit diversity in *Ficus* (Moraceae). *Proc Natl Acad Sci USA* 107:14668–14672.
17. Guimarães PR, Jordano P, Thompson JN (2011) Evolution and coevolution in mutualistic networks. *Ecol Lett* 14:877–885.
18. Fonseca CR, Ganade G (1996) Asymmetries, compartments and null interactions in an Amazonian ant-plant community. *J Anim Ecol* 65:339–347.
19. Ricciardi F, Boyer M, Ollerton J (2010) Assemblage and interaction structure of the anemonefish-anemone mutualism across the Manado region of Sulawesi, Indonesia. *Environ Biol Fishes* 87:333–347.
20. Orona-Tamayo D, et al. (2013) Exclusive rewards in mutualisms: Ant proteases and plant protease inhibitors create a lock-key system to protect Acacia food bodies from exploitation. *Mol Ecol* 22:4087–4100.
21. Gomulkiewicz R, Thompson JN, Holt RD, Nuismer SL, Hochberg ME (2000) Hot spots, cold spots, and the geographic mosaic theory of coevolution. *Am Nat* 156:156–174.
22. Kalske A, Leimu R, Scheepens JF, Mutikainen P (2016) Spatiotemporal variation in local adaptation of a specialist insect herbivore to its long-lived host plant. *Evolution* 70:2110–2122.
23. Thompson JN, Schwind C, Friberg M (2017) Diversification of trait combinations in coevolving plant and insect lineages. *Am Nat* 190:171–184.
24. Vogwill T, Fenton A, Buckling A, Hochberg ME, Brockhurst MA (2009) Source populations act as coevolutionary pacemakers in experimental selection mosaics containing hotspots and coldspots. *Am Nat* 173:E171–E176.
25. Toju H, Ueno S, Taniguchi F, Sota T (2011) Metapopulation structure of a seed-predator weevil and its host plant in arms race coevolution. *Evolution* 65:1707–1722.
26. Yoder JB, et al. (2013) Effects of gene flow on phenotype matching between two varieties of Joshua tree (*Yucca brevifolia*; Agavaceae) and their pollinators. *J Evol Biol* 26:1220–1233.
27. Lion S, Gandon S (2015) Evolution of spatially structured host-parasite interactions. *J Evol Biol* 28:10–28.
28. Fitzpatrick SW, Gerberich JC, Kronenberger JA, Angeloni LM, Funk WC (2015) Locally adapted traits maintained in the face of high gene flow. *Ecol Lett* 18:37–43.
29. Urban MC, et al. (2008) The evolutionary ecology of metacommunities. *Trends Ecol Evol* 23:311–317.
30. Toju H, et al. (2017) Species-rich networks and eco-evolutionary synthesis at the metacommunity level. *Nat Ecol Evol* 1:0024.
31. Emer C, et al. (2018) Seed-dispersal interactions in fragmented landscapes—A metanetwork approach. *Ecol Lett* 21:484–493.
32. Jacob S, et al. (2017) Gene flow favours local adaptation under habitat choice in ciliate microcosms. *Nat Ecol Evol* 1:1407–1409.
33. Olesen JM, Bascompte J, Dupont YL, Jordano P (2007) The modularity of pollination networks. *Proc Natl Acad Sci USA* 104:19891–19896.
34. Brouat C, Garcia N, Andary C, McKee D (2001) Plant lock and ant key: Pairwise coevolution of an exclusion filter in an ant-plant mutualism. *Proc Biol Sci B* 268:2131–2141.
35. Elias M, Gompert Z, Jiggins C, Willmott K (2008) Mutualistic interactions drive ecological niche convergence in a diverse butterfly community. *PLoS Biol* 6:2642–2649.
36. Haddad NM, et al. (2015) Habitat fragmentation and its lasting impact on earth's ecosystems. *Sci Adv* 1:e1500052.
37. Aguilar R, Quesada M, Ashworth L, Herreras-Diego Y, Lobo J (2008) Genetic consequences of habitat fragmentation in plant populations: Susceptible signals in plant traits and methodological approaches. *Mol Ecol* 17:5177–5188.
38. Schleuning M, Fründ J, García D (2015) Predicting ecosystem functions from biodiversity and mutualistic networks: An extension of trait-based concepts to plant-animal interactions. *Ecosystems* 38:380–392.
39. Almeida-Neto M, Guimarães P, Guimarães PR, Loyola RD, Ulrich W (2008) A consistent metric for nestedness analysis in ecological systems: Reconciling concept and measurement. *Oikos* 117:1227–1239.
40. Marquitti FMD, Guimarães PR, Pires MM, Bittencourt LF (2014) MODULAR: Software for the autonomous computation of modularity in large network sets. *Ecosystems* 37:221–224.

# Supporting Information: The geographic mosaic of coevolution in mutualistic networks

Lucas P. Medeiros, Guilherme Garcia, John N. Thompson & Paulo R. Guimarães Jr.

## Contents

|   |           |
|---|-----------|
| <b>1 Coevolutionary models</b>  | <b>2</b>  |
| 1.1 Single-site coevolutionary model  | 2         |
| 1.2 Two-site coevolutionary model   | 3         |
| <b>2 Gene flow, geographical variation in selection and the evolution of trait patterns</b> | <b>4</b>  |
| 2.1 Numerical simulations   | 4         |
| 2.1.1 Single-site coevolutionary model  | 5         |
| 2.1.2 Two-site coevolutionary model   | 6         |
| 2.1.3 Effect of gene flow on pairwise trait matching  | 6         |
| 2.1.4 Effect of gene flow on environmental matching and geographical divergence             | 7         |
| 2.1.5 Simulations with different parameterizations  | 7         |
| 2.1.6 Simulations with gene flow correlated with species degree                             | 9         |
| 2.1.7 Simulations with spatial species turnover   | 9         |
| 2.2 Analytical approximations   | 10        |
| 2.2.1 Single-site coevolutionary model  | 10        |
| 2.2.2 Two-site coevolutionary model   | 11        |
| 2.2.3 Matrix $\mathbf{T}$ and the emergence of trait matching                               | 13        |
| <b>3 Network structure and the evolution of trait patterns</b>                              | <b>14</b> |
| 3.1 Network structure metrics   | 14        |
| 3.2 Principal Component Analysis  | 15        |
| <b>4 Disruption of gene flow and its consequences for coevolution</b>                       | <b>15</b> |
| <b>5 Figures and tables</b>   | <b>21</b> |

# 1 Coevolutionary models

## 1.1 Single-site coevolutionary model

Here we present the details of the single-site coevolutionary model, which was developed by (1). In this single-site model, we represented each of the  $N$  species that are part of a mutualistic network as a single population. We modeled the evolution of the mean value of a single trait of each species ( $z_i$ ) by explicitly defining the selection gradient that drives evolutionary change. We assumed that population sizes are large enough for genetic drift to be negligible. We also assumed that the phenotypic variance of the trait ( $\sigma_{z_i}^2$ ) is fixed through time, which is a reasonable approximation if population sizes are large and selection does not modify the genetic variance. We considered that  $z_i$  mediates mutualistic interactions between individuals (e.g., flower tube length, pollinator mouthpart length) and affects the fitness benefits of mutualism. In addition to mutualism,  $z_i$  also determines fitness components related to abiotic factors and other ecological interactions (2, 3). Thus,  $z_i$  is under selection imposed by mutualism (hereafter mutualistic selection) and selection imposed by abiotic factors and other ecological interactions (hereafter environmental selection).

The change in the mean trait value of species  $i$  between generation  $t$  and generation  $t + 1$  was derived using the classical equation by (4):

$$z_i^{(t+1)} = z_i^{(t)} + h_{z_i}^2 \sigma_{z_i}^2 \frac{\partial \ln W_i}{\partial z_i^{(t)}} \quad [S1]$$

where  $h_{z_i}^2$  ( $0 \leq h_{z_i}^2 \leq 1$ ) is the heritability of the trait of species  $i$  that we assumed to be constant over time and  $\frac{\partial \ln W_i}{\partial z_i^{(t)}}$  is the selection gradient. We assumed that the adaptive landscape of each species, defined by mutualistic and environmental selection, has a single adaptive peak at each generation. We incorporated temporal variation in the adaptive peaks, which were reshaped over time by the trait evolution of all species in the mutualistic assemblage. To do so, we defined a linear selection gradient as follows:

$$\frac{\partial \ln W_i}{\partial z_i^{(t)}} = \rho_i [z_{i,p}^{(t)} - z_i^{(t)}] \quad [S2]$$

in which  $\rho_i$  is a scaling constant that relates changes in mean fitness to changes in mean trait values and  $z_{i,p}^{(t)}$  is the trait value that defines the adaptive peak of the population at generation  $t$ . We decomposed  $z_{i,p}^{(t)}$  into two components, one related to mutualism and one related to the environment:

$$z_{i,p}^{(t)} = \sum_{j=1}^N q_{ij}^{(t)} x_{ij}^{(t)} + (1 - \sum_{j=1}^N q_{ij}^{(t)}) \theta_i \quad [S3]$$

In the equation above,  $q_{ij}^{(t)}$  is the interaction weight that describes the evolutionary effect of species  $j$  on the selection gradient of species  $i$  ( $0 \leq q_{ij}^{(t)} \leq 1$ ). We defined that the sum of all evolutionary effects acting on a species is equal to the relative importance of mutualism as a selective pressure (i.e.  $0 \leq \sum_{j=1}^N q_{ij}^{(t)} = m_i \leq 1$ ). Thus, parameter  $m_i$  denotes the level of mutualistic selection and the term  $(1 - \sum_{j=1}^N q_{ij}^{(t)}) = (1 - m_i)$  represents the level of environmental selection. Finally,  $x_{ij}^{(t)}$  is the trait value of species  $i$  favored by selection imposed by species  $j$  and  $\theta_i$  is the trait value favored by environmental selection, which we assumed to be fixed over time.

We used one additional assumption to obtain a final equation describing the dynamics of trait  $z_i$  at a single site. We supposed that mutualistic selection favors the complementarity of traits, i.e., phenotype matching (5, 2, 3). Thus, the selected trait value with respect to partner  $j$  at generation  $t$  is  $x_{ij}^{(t)} = z_j^{(t)}$ ,

which corresponds to the value that maximizes the trait matching between  $z_i$  and  $z_j$ . Using equations [S1], [S2], and [S3] and the fact that  $h_{z_i}^2 = \frac{\sigma_{G_{z_i}}^2}{\sigma_{z_i}^2}$ , in which  $\sigma_{G_{z_i}}^2$  is the additive genetic variance of trait  $z_i$ , the dynamics of trait  $z_i$  may be described as follows (1):

$$z_i^{(t+1)} = z_i^{(t)} + \varphi_i \left[ \sum_{j=1}^N q_{ij}^{(t)} (z_j^{(t)} - z_i^{(t)}) + (1 - \sum_{j=1}^N q_{ij}^{(t)}) (\theta_i - z_i^{(t)}) \right] \quad [\text{S4}]$$

in which  $\varphi_i$  is a compound parameter that depends on the additive genetic variance of the trait and on the slope of the selection gradient ( $\varphi_i = \sigma_{G_{z_i}}^2 \rho_i$ ).

We now describe how  $q_{ij}^{(t)}$ , which represents the evolutionary effect of species  $j$  on species  $i$  in relation to all other mutualistic partners of  $i$ , changes through time. The term  $q_{ij}^{(t)}$  has two components that represent how different traits mediate the fitness consequences of the interaction with species  $j$ . The first component is related to trait  $z_i$  and is given by the trait matching between  $z_i$  and  $z_j$ , which we defined using a gaussian function as:

$$\tau_{ij}^{(t)} = e^{-\alpha(z_j^{(t)} - z_i^{(t)})^2} \quad [\text{S5}]$$

where the parameter  $\alpha$  controls the sensitivity of  $\tau_{ij}^{(t)}$  to differences between traits and was assumed to be the same for every species and to be fixed over time. The value of  $\tau_{ij}^{(t)}$  is 1 when there is maximum matching ( $z_j^{(t)} = z_i^{(t)}$ ) and approximates 0 if trait matching is poor. This gaussian function is widely used in coevolutionary models to represent trait matching (1, 2, 3, 6). The second component is the binary term  $a_{ij}^{(t)}$ , which encapsulates the effects of a suite of other traits not explicitly modeled by us and defines if an interaction is allowed to occur ( $a_{ij}^{(t)} = 1$ ) or represents an evolutionary forbidden link ( $a_{ij}^{(t)} = 0$ ) (7). We assumed that  $z_i$  evolves at a faster rate than all other traits associated with the interaction and, therefore,  $a_{ij}^{(t)}$  may be considered fixed (i.e.,  $a_{ij}^{(t)} = a_{ij}$ ). We also assumed that the genetic covariance between  $z_i$  and other traits related to the mutualism is negligible, which allowed us to consider these two components independently. The combination of the two components leads to:

$$q_{ij}^{(t)} = m_i \frac{a_{ij} \tau_{ij}^{(t)}}{\sum_{k=1}^N a_{ik} \tau_{ik}^{(t)}} \quad [\text{S6}]$$

In our simulations, we parameterized  $a_{ij}$  and species richness ( $N$ ) using the binary adjacency matrices  $\mathbf{A}$  of our dataset (Table S1). In matrix  $\mathbf{A}$  ( $N \times N$ ), the row and column  $i$  represent species  $i$  and the binary element  $a_{ij}$  indicates if species  $i$  and  $j$  interact in the mutualistic assemblage. Therefore, matrix  $\mathbf{A}$  imposes a fixed structure of potential interactions, whereas  $q_{ij}^{(t)}$  changes through time and defines a dynamic structure of the evolutionary strength of interactions.

## 1.2 Two-site coevolutionary model

We extended the single-site coevolutionary model to a two-site model in order to incorporate simple geographical variation in selection and gene flow. In our two-site model, one population of each species occurs in each site, with  $N_A$  species at site  $A$  and  $N_B$  species at site  $B$ . At each site, species engage in mutualistic interactions, forming a local mutualistic network. We considered that, after selection operates at generation  $t$ , a fraction  $g_i^{(t)}$  of the population of species  $i$  migrates from site  $A$  to site  $B$  and from site  $B$  to site  $A$  and a fraction  $(1 - g_i^{(t)})$  remains at its own site. Therefore, we supposed that migration is symmetric between sites, which would not alter population sizes through time. We also assumed that migration ability

is a fixed property of each species and does not change over time, which allowed us to set  $g_i^{(t)} = g_i$ . Finally, we assumed that local individuals and migrants mate randomly, which allowed us to use  $g_i$  as a measure of gene flow. Thus, our two-site model describes coevolutionary dynamics in a metanetwork (8, 9) consisting of two local mutualistic networks connected by gene flow. These assumptions allowed us to implement gene flow as a process that mixes trait values across sites, as in other coevolutionary models (e.g., (2)), leading to the following equation for the change in trait  $z_{i,A}$  of species  $i$  at site  $A$ :

$$z_{i,A}^{(t+1)} = (1 - g_i)(z_{i,A}^{(t)} + \delta_{z_{i,A}}^{(t)}) + g_i(z_{i,B}^{(t)} + \delta_{z_{i,B}}^{(t)}) \quad [S7]$$

where  $\delta_{z_{i,A}}^{(t)}$  and  $\delta_{z_{i,B}}^{(t)}$  are the evolutionary changes for both population of species  $i$  as defined in equation [S4]:

$$\delta_{z_{i,A}}^{(t)} = \varphi_{i,A} \left[ \sum_{j=1}^{N_A} q_{ij,A}^{(t)} (z_{j,A}^{(t)} - z_{i,A}^{(t)}) + (1 - \sum_{j=1}^{N_A} q_{ij,A}^{(t)}) (\theta_{i,A} - z_{i,A}^{(t)}) \right] \quad [S8]$$

$$\delta_{z_{i,B}}^{(t)} = \varphi_{i,B} \left[ \sum_{j=1}^{N_B} q_{ij,B}^{(t)} (z_{j,B}^{(t)} - z_{i,B}^{(t)}) + (1 - \sum_{j=1}^{N_B} q_{ij,B}^{(t)}) (\theta_{i,B} - z_{i,B}^{(t)}) \right] \quad [S9]$$

All model parameters have the same definitions as in the single-site coevolutionary model and  $q_{ij,A}^{(t)}$  and  $q_{ij,B}^{(t)}$  are defined as in equations [S5] and [S6]. Most of the analyses described in the next sections are restricted to the case in which both sites have the same species composition ( $N_A = N_B = N$ ) and mutualistic network (matrix  $\mathbf{A}$ ). These analyses allowed us to gain insight into how species coevolve under simple spatial scenarios by deriving the evolutionary dynamics from first principles and without the complicating effects of spatial turnover in species composition and mutualistic interactions. However, because spatial turnover is observed in many spatial studies of mutualistic networks (10, 11, 9), we performed sensitivity analyses in which species composition and mutualistic interactions vary across sites. Furthermore, in all of our analyses, the parameters  $\varphi_i$ ,  $m_i$ , and  $\theta_i$  could be different for the two populations of each species  $i$ , generating distinct local adaptive landscapes for each population. This allowed us to explore the main focus of this study: how geographical variation in mutualistic selection ( $m_{i,A}$  and  $m_{i,B}$ ) and gene flow ( $g_i$ ) may affect trait evolution in mutualistic networks.

## 2 Gene flow, geographical variation in selection and the evolution of trait patterns

### 2.1 Numerical simulations

We performed numerical simulations of our two-site coevolutionary model to understand how gene flow ( $g_i$ ) and geographical variation in mutualistic selection ( $m_{i,A}$  and  $m_{i,B}$ ) affect trait evolution. Simulations and analyses were performed in R 3.3.2 (12) and all codes are available at [www.github.com/wgar84/spatial\\_coevo\\_mutnet](https://www.github.com/wgar84/spatial_coevo_mutnet). Our first step in performing simulations was to choose a mutualistic assemblage and to parameterize the number of species ( $N$ ) and the adjacency matrix  $\mathbf{A}$  (i.e.,  $a_{ij}$  values) using the empirical information (Table S1). Next, we sampled initial trait values ( $z_{i,A}^{(0)}$  and  $z_{i,B}^{(0)}$ ) and parameter values ( $m_{i,A}$ ,  $m_{i,B}$ ,  $g_i$ ,  $\theta_{i,A}$ ,  $\theta_{i,B}$ ,  $\varphi_{i,A}$ ,  $\varphi_{i,B}$ ) for each species at both sites from statistical distributions (Table S2). Therefore, except for the parameter  $\alpha$ , which was the same for all species, we incorporated variation in parameter values across species and across sites. We then iterated equation [S7] until changes in trait values were less than

$10^{-6}$  (i.e.,  $|z_{i,A}^{(t+1)} - z_{i,A}^{(t)}| < 10^{-6}$  and  $|z_{i,B}^{(t+1)} - z_{i,B}^{(t)}| < 10^{-6}$ ). This threshold was more than sufficient for traits to reach equilibrium values (Fig. S1). For each simulation, we recorded trait values through time and calculated trait matching ( $\tau_{ij}^{(t)}$ ) using equation [S5] and setting the constant  $\alpha$  to 0.2. We used  $\tau_{ij}^{(t)}$  as our metric for trait matching because it is linked to our coevolutionary model and because it is correlated with another trait matching metric that is also based on differences between traits of interacting partners (13). We also calculated the mean trait matching for all interacting species pairs as:

$$\bar{\tau}^{(t)} = \frac{\sum_{i=1}^N \sum_{j=1}^N a_{ij} \tau_{ij}^{(t)}}{\sum_{i=1}^N \sum_{j=1}^N a_{ij}} \quad [\text{S10}]$$

We performed simulations according to several different scenarios in order to extensively explore the parameter space. In the main text, we report the results of our two main scenarios of geographical variation in selection, which consist of two hotspots ( $\bar{m}_A = \bar{m}_B = 0.7$ ) and a hotspot and a coldspot ( $\bar{m}_A = 0.9$  and  $\bar{m}_B = 0.1$ ). Here, we report the simulation results of our complete set of 15 combinations of  $\bar{m}_A$  and  $\bar{m}_B$  (Table S2, Fig. S2). For each combination of  $\bar{m}_A$  and  $\bar{m}_B$ , we explored 31 different values of gene flow ( $\bar{g} = 0, 0.01, 0.02, \dots, 0.28, 0.29, 0.3$ ). For each combination of mutualistic selection and gene flow, we performed 100 simulations per empirical network ( $n = 72$  networks, total = 3,348,000 simulations). Note that, when  $\bar{g} = 0$ , the two-site coevolutionary model (eq. [S7]) becomes identical to the single-site model (eq. [S4]), which allowed us to explore the coevolutionary dynamics of isolated sites as well (see below). These simulations allowed us to investigate how trait patterns emerge in mutualistic networks in several distinct scenarios of geographical variation in selection and gene flow across sites.

Although the scenarios outlined above allowed us to explore how gene flow and geographical variation in selection affect the emergence of trait patterns, other parameters may affect trait evolution. In the main text, we showed how network properties contained in the adjacency matrix  $\mathbf{A}$  affect the emergence of trait matching (Fig. 3). Here, we report additional evidence that network structure modulates the effects of gene flow and mutualistic selection on trait evolution (Fig. S2, S3). Furthermore, we present simulation results for other parameterizations for  $\theta_{i,A}, \theta_{i,B}, \varphi_{i,A}, \varphi_{i,B}$ , and  $\alpha$  (Table S2; see *Simulations with different parameterizations*), and for two other situations: when gene flow is correlated with the number of interactions of each species (see *Simulations with gene flow correlated with species degree*) and when there is spatial species turnover (see *Simulations with spatial species turnover*). We show that the majority of these other parameterizations do not qualitatively change our main conclusions of how gene flow affects the emergence of trait matching (Fig. S5, S6, S7).

### 2.1.1 Single-site coevolutionary model

We performed simulations without gene flow (i.e.,  $\bar{g} = 0$ ) and with the same parameter choices of the main text (Table S2) to understand how mutualistic selection ( $\bar{m}$ ) affects the strength of reciprocal selection and the emergence of trait matching throughout the simulations (Fig. S1). We measured the reciprocity of selection between mutualistic partners  $i$  and  $j$  at time  $t$  using the pairwise evolutionary effects between these two species (eq. [S6]). We calculated the reciprocity of selection in log to avoid multiplying  $q_{ij}^{(t)}$  values close to zero:

$$\log(r_{ij}^{(t)}) = \log\left(\frac{q_{ij}^{(t)}}{m_i}\right) + \log\left(\frac{q_{ji}^{(t)}}{m_j}\right) \quad [\text{S11}]$$

Higher values of  $\log(r_{ij}^{(t)})$  indicate that the selective pressures that species  $i$  and  $j$  exert on each other are more reciprocal. We calculated the mean reciprocity of selection for all pairs of species in the network ( $\log(\bar{r}^{(t)})$ ) through time for each simulation.

We found that higher values of mutualistic selection lead to stronger reciprocal selection (Fig. S1A) and to higher values of trait matching over time (Fig. S1B). These results allowed us to define a site with a high value of  $\bar{m}$  as a hotspot and a site with a low value of  $\bar{m}$  as a coldspot. Furthermore, these results served as a baseline for our results of the two-site coevolutionary model (see below).

### 2.1.2 Two-site coevolutionary model

In addition to the two combinations of mutualistic selection presented in the main text ( $\bar{m}_A = \bar{m}_B = 0.7$  and  $\bar{m}_A = 0.9, \bar{m}_B = 0.1$ ), we performed simulations using 13 other combinations of mutualistic selection (Table S2). Our results indicate that higher values of gene flow ( $\bar{g}$ ) favor higher levels of trait matching at equilibrium ( $\bar{\tau}^*$ ) for most scenarios of geographical variation in mutualistic selection (Fig. S2). However, increasing gene flow causes trait matching to decrease in a hotspot when it is connected to a coldspot (e.g.,  $\bar{m}_A = 0.9, \bar{m}_B = 0.1$ , Fig. S2).

### 2.1.3 Effect of gene flow on pairwise trait matching

Our previous results show that gene flow may cause the mean trait matching among all interacting species to increase in mutualistic networks (Fig. S2). We now present our results of how gene flow affects the evolution of trait matching in different pairs of interacting species. We first calculated the number of interactions (or degree) of each species  $i$  in a network as  $k_i = \sum_{j=1}^N a_{ij}$ . We then explored how gene flow affects the trait matching between species  $i$  and  $j$  ( $\tau_{ij}^{(t)}$ ) depending on the degree of both species (i.e.,  $k_i$  and  $k_j$ ). By doing so, we aimed to understand how gene flow affects the coevolutionary dynamics of mutualistic partners when the number of selective pressures acting upon the two interacting species (i.e., number of additional interaction partners) varies. We measured the equilibrium value of trait matching ( $\bar{\tau}_{ij}^*$ ) for every pair of species in our simulations using the complete dataset (72 empirical networks, 7,239 pairs of species). We computed ( $\bar{\tau}_{ij}^*$ ) using the results of our two main scenarios of mutualistic selection ( $\bar{m}_A = \bar{m}_B = 0.7$  and  $\bar{m}_A = 0.9, \bar{m}_B = 0.1$ ) with and without gene flow ( $\bar{g} = 0.3$  and  $\bar{g} = 0$ , respectively). Because we performed 100 simulations per network for every combination of  $\bar{m}_A$ ,  $\bar{m}_B$ , and  $\bar{g}$ , we calculated the average value of equilibrium trait matching for each pair of species across the 100 simulations ( $\bar{\tau}_{ij}^*$ ). Note that  $\bar{\tau}_{ij}^*$  is different from  $\bar{\tau}^*$  (eq. [S10]), which is the mean equilibrium trait matching for all pairs of species in a given network. Our final step was to calculate the difference between the mean pairwise trait matching with gene flow and without gene flow ( $\bar{\tau}_{ij,g=0.3}^* - \bar{\tau}_{ij,g=0}^*$ ) for each pair of species  $i$  and  $j$ .

Our results show that the higher the degree of both interacting species, the greater the difference between pairwise trait matching with ( $\bar{\tau}_{ij,g=0.3}^*$ ) and without gene flow ( $\bar{\tau}_{ij,g=0}^*$ , Fig. S3). In two hotspots ( $\bar{m}_A = \bar{m}_B = 0.7$ ), pairs of specialist species (i.e., both species have low degree values) evolve high levels of trait matching in the presence or absence of gene flow (Fig. 2). Pairs of generalist species (i.e., both species have high degree values), on the other hand, evolve high levels of trait matching only in the presence of gene flow (Fig. 2). Hence, pairs of generalist species show greater differences in trait matching with and without gene flow than pairs of specialist species (Fig. S3A). In a hotspot and a coldspot ( $\bar{m}_A = 0.9$  and  $\bar{m}_B = 0.1$ ), we also observe a greater difference in pairwise trait matching for pairs of generalist species (Fig. S3B). However, because trait matching values in the hotspot (i.e., site  $A$ ) are higher in the absence of gene flow, differences in pairwise trait matching with and without gene flow are negative for this scenario (Fig. S3B). These results

demonstrate that the changes we observe in mean trait matching ( $\bar{\tau}^*$ ) as we increase gene flow (Fig. 2, Fig. S2) are a consequence of changes in pairwise trait matching among generalist species.

#### 2.1.4 Effect of gene flow on environmental matching and geographical divergence

In our simulations of the two-site coevolutionary model, we also measured how well matched species traits are to the value selected by the local environment ( $\theta_{i,A}$  or  $\theta_{i,B}$ ) and how divergent are the traits of the two populations of the same species ( $z_{i,A}^{(t)}$  and  $z_{i,B}^{(t)}$ ). We used our expression for trait matching (eq. [S5]) to calculate these two quantities, which we called environmental matching and geographical divergence, respectively. The environmental matching of trait  $z_{i,A}^{(t)}$  at generation  $t$  was calculated as:

$$\varepsilon_{i,A}^{(t)} = e^{-\alpha(\theta_{i,A} - z_{i,A}^{(t)})^2} \quad [\text{S12}]$$

where  $\alpha$  is a constant set to 0.2. We calculated  $\varepsilon_{i,B}^{(t)}$  using equation [S12] with subscript  $B$  instead of  $A$ . The value of  $\varepsilon_{i,A}^{(t)}$  ( $\varepsilon_{i,B}^{(t)}$ ) is 1 when trait  $z_{i,A}^{(t)}$  ( $z_{i,B}^{(t)}$ ) is completely coupled with its local environmental optimum and it approaches 0 when the trait value is very far from  $\theta_{i,A}$  ( $\theta_{i,B}$ ). The geographical divergence of the trait of species  $i$  at generation  $t$  was calculated as:

$$\gamma_i^{(t)} = e^{-\alpha(z_{i,B}^{(t)} - z_{i,A}^{(t)})^2} \quad [\text{S13}]$$

where  $\alpha$  was also set to 0.2. The value of  $\gamma_i^{(t)}$  is 1 when both traits have the same value (i.e.,  $z_{i,A}^{(t)} = z_{i,B}^{(t)}$ ) and it approaches 0 when  $z_{i,A}^{(t)}$  and  $z_{i,B}^{(t)}$  are very different from each other. In addition to calculating the environmental matching and geographical divergence for each species, we also quantified these metrics for the entire network by taking the average across all species ( $\bar{\varepsilon}_A^{(t)}$ ,  $\bar{\varepsilon}_B^{(t)}$ ,  $\bar{\gamma}^{(t)}$ ). We computed the equilibrium values of the mean environmental matching and mean geographical divergence ( $\bar{\varepsilon}_A^*$ ,  $\bar{\varepsilon}_B^*$ , and  $\bar{\gamma}^*$ ) for all our simulations using our two main scenarios of mutualistic selection ( $\bar{m}_A = \bar{m}_B = 0.7$  and  $\bar{m}_A = 0.9$ ,  $\bar{m}_B = 0.1$ ) and all values of gene flow ( $\bar{g} = 0, 0.01, \dots, 0.29, 0.3$ ).

We found that the mean environmental matching at equilibrium decreases as gene flow increases irrespective of the values of mutualistic selection (Fig. S4A). This result confirms our expectation that gene flow reduces the local adaptation of each population to its local environment by mixing the phenotypes of distinct populations. Furthermore, we found that the mean geographical divergence at equilibrium also decreases as gene flow increases for both combinations of mutualistic selection (Fig. S4B). Thus, as expected, gene flow causes the trait values of different populations of the same species to become more similar to each other. By causing species traits to move away from their local environmental optima and to become homogeneous across sites, gene flow allows mutualistic selection to gain importance and trait matching to increase (Fig. 2, Fig. S2).

#### 2.1.5 Simulations with different parameterizations

In this first set of sensitivity analyses, we performed simulations to investigate how the parameters  $\theta_{i,A}$ ,  $\theta_{i,B}$ ,  $\varphi_{i,A}$ ,  $\varphi_{i,B}$ , and  $\alpha$  affect trait evolution in mutualistic networks across space. In these analyses, we changed the value or sampling distribution of one parameter while maintaining the other parameters unchanged. In our main set of simulations, presented above and in the main text, we sampled  $\theta_{i,A}$  from a uniform distribution between 0 and 10,  $\theta_{i,B}$  from a uniform distribution between 10 and 20,  $\varphi_{i,A}$  and  $\varphi_{i,B}$  both from a normal distribution with mean 0.5, and  $\alpha$  was set to 0.2 (Table S2). Here, we present simulation

results for four additional parameterizations for  $\theta_{i,A}$  and  $\theta_{i,B}$ , two additional parameterizations for  $\varphi_{i,A}$  and  $\varphi_{i,B}$ , and two additional parameterizations for  $\alpha$  (Table S2). In these additional simulations, we used two combinations of mutualistic selection ( $\bar{m}_A = \bar{m}_B = 0.7$  and  $\bar{m}_A = 0.9, \bar{m}_B = 0.1$ ) and 13 values of gene flow ( $\bar{g} = 0, 0.025, 0.05, \dots, 0.25, 0.275, 0.3$ ). We used a random sample of 36 empirical networks of our complete dataset (Table S1), but established a priori that our sample would include all types of mutualism and would have a variation in network structure similar to our complete dataset (Table S1). For each combination of  $\bar{m}_A, \bar{m}_B, \bar{g}, \theta_{i,A}, \theta_{i,B}, \varphi_{i,A}, \varphi_{i,B}$ , and  $\alpha$  we performed 50 simulations per empirical network ( $n = 36$  networks, total = 374,400 simulations).

We first present our results for the different parameterizations of  $\theta_{i,A}$  and  $\theta_{i,B}$ . In our main parameterization ( $\theta_{i,A} \sim \mathcal{U}[0, 10], \theta_{i,B} \sim \mathcal{U}[10, 20]$ ), we assumed that environmental factors select for lower trait values at site  $A$  than at site  $B$ . Such geographical variation in environmental selection is observed for many systems of interacting species (14, 15, 16, 17). In our first additional parameterization, we assumed that the environmental optima have the same distribution at both sites ( $\theta_{i,A} \sim \mathcal{U}[0, 10], \theta_{i,B} \sim \mathcal{U}[0, 10]$ ). In our second additional parameterization, we assumed that site  $A$  select for lower trait values than site  $B$ , but the distributions of environmental optima overlap ( $\theta_{i,A} \sim \mathcal{U}[0, 10], \theta_{i,B} \sim \mathcal{U}[5, 15]$ ). In our third additional parameterization, we assumed that site  $A$  select for much lower trait values than site  $B$  ( $\theta_{i,A} \sim \mathcal{U}[0, 10], \theta_{i,B} \sim \mathcal{U}[20, 30]$ ). Importantly,  $\theta_{i,A}$  and  $\theta_{i,B}$  are sampled independently in all the parameterizations described so far.

Our results for these three additional parameterizations show that the mean distance between the two distributions ( $\theta_{i,A}$  and  $\theta_{i,B}$ ) does not affect our conclusions of how gene flow and geographical variation in mutualistic selection influence trait matching (Fig. S5A-C). Although the variance of the distribution could affect our results, we show below by changing the value of  $\alpha$  that this is not the case. Finally, in our fourth additional parameterization, we assumed that there is a correlation between the trait values selected at site  $A$  and those selected at site  $B$ , that is,  $\theta_{i,A}$  and  $\theta_{i,B}$  were not sampled independently. For these simulations, we sampled environmental optima for site  $A$  ( $\theta_{i,A} \sim \mathcal{U}[0, 10]$ ) and we defined environmental optima for site  $B$  as  $\theta_{i,B} = \theta_{i,A} + \mathcal{N}[\mu = 10, \sigma^2 = 1]$ . Using this sampling procedure, the mean correlation between  $\theta_{i,A}$  and  $\theta_{i,B}$  values was 0.944 ( $n = 46,800$  simulations). Our simulations using this fourth parameterization showed that gene flow does not favor trait matching when  $\theta_{i,A}$  and  $\theta_{i,B}$  are highly correlated (Fig. S5D). Given indirect coevolutionary effects (1), we can interpret  $\theta_{i,A}$  and  $\theta_{i,B}$  values as key components of the local selection regime of each species in the network. Our results show that gene flow favors trait matching only when the selection regime of each species varies geographically (i.e.,  $\theta_{i,A}$  and  $\theta_{i,B}$  are uncorrelated).

We now present our results for the different parameterizations of  $\varphi_{i,A}$  and  $\varphi_{i,B}$ . In our main parameterization, we assumed that the distribution of  $\varphi_{i,A}$  and  $\varphi_{i,B}$  is the same for both sites and we sampled these parameters from a normal distribution ( $\mathcal{N}[\mu = 0.5, \sigma^2 = 0.0001]$ ). We performed simulations using two additional parameterizations in which we set the mean of the normal distribution to 0.1 and 1 (Table S2). These simulations show that different parameterizations for  $\varphi_{i,A}$  and  $\varphi_{i,B}$  do not change our conclusions about how gene flow and mutualistic selection affect trait matching (Fig. S5E, F). Therefore, although  $\varphi_{i,A}$  and  $\varphi_{i,B}$  have an effect on the speed of the coevolutionary dynamics (1), these parameters do not affect the emergence of trait matching.

Finally, we also performed simulations with different parameterizations for  $\alpha$ . In our main parameterization, we assumed that  $\alpha$  is the same for every species and is fixed over time and we set the value of this parameter to 0.2. We performed simulations using two additional parameterizations in which we set the value of  $\alpha$  to 0.05 and 0.8 (Table S2). Note that multiplying trait differences (i.e.,  $z_j^{(t)} - z_i^{(t)}$ ) by a constant  $c$  has

the same effect on trait matching (eq. [S5]) as multiplying  $\alpha$  by  $c^2$ , because:

$$e^{-\alpha[c(z_j^{(t)} - z_i^{(t)})]^2} = e^{-(\alpha c^2)(z_j^{(t)} - z_i^{(t)})^2} \quad [\text{S14}]$$

Therefore, because trait values ( $z_{i,A}^{(t)}$  and  $z_{i,B}^{(t)}$ ) in our simulations follow the same distribution as  $\theta_{i,A}$  and  $\theta_{i,B}$ , respectively (Table S2), changing  $\alpha$  has the same effect on trait matching as modifying the range of  $\theta_{i,A}$  and  $\theta_{i,B}$  values. In particular, by multiplying  $\alpha = 0.2$  by  $\frac{1}{4}$  to obtain  $\alpha = 0.05$  and by 4 to obtain  $\alpha = 0.8$ , we are also testing the effect of shrinking and expanding, respectively, the range of both  $\theta_{i,A}$  and  $\theta_{i,B}$  by 2. Our simulations parameterized by  $\alpha = 0.05$  and  $\alpha = 0.8$  show that different values of  $\alpha$  do not change our results of how gene flow affect trait matching (Fig. S5G, H). Hence, our main conclusions of how gene flow and geographic variation in selection affect trait matching are robust to several changes in the parameters of our coevolutionary model.

### 2.1.6 Simulations with gene flow correlated with species degree

In this second set of sensitivity analyses, we explored how the correlation between gene flow ( $g_i$ ) and the number of interactions of each species, (species degree,  $k_i$ ) may affect our previous results. To do so, we performed simulations in which we imposed the highest possible positive correlation between the vector of gene flow values ( $g_1, g_2, \dots, g_N$ ) and the vector of species degree values ( $k_1, k_2, \dots, k_N$ ) by aligning the two ordered vectors before simulating the coevolutionary dynamics. These simulations allowed us to explore a scenario in which generalist species are locally more abundant than specialist species (18) and, therefore, have more individuals migrating across sites. In these simulations, we used two combinations of mutualistic selection ( $\bar{m}_A = \bar{m}_B = 0.7$  and  $\bar{m}_A = 0.9, \bar{m}_B = 0.1$ ) and 13 values of gene flow ( $\bar{g} = 0, 0.025, 0.05, \dots, 0.25, 0.275, 0.3$ ). In order to better explore the association between gene flow and species degree, we introduced a larger variation in gene flow values across species in these simulations than in previous simulations (Table S2). Finally, we used a random sample of 36 empirical networks of our complete dataset (Table S1). For each combination of  $\bar{m}_A$ ,  $\bar{m}_B$ , and  $\bar{g}$  we performed 50 simulations per empirical network ( $n = 36$  networks, total = 46,800 simulations).

In the simulations with gene flow (i.e.,  $\bar{g} > 0$ ), the mean value of Spearman's rank correlation between gene flow and species degree was  $0.92 \pm 0.07$  (mean  $\pm$  sd,  $n = 43,200$ ). Our results show that the effect of gene flow on the emergence of trait matching does not change when we impose a positive correlation between gene flow and species degree (Fig. S6).

### 2.1.7 Simulations with spatial species turnover

In this final set of sensitivity analyses, we investigated the effects of spatial species turnover on the emergence of trait matching in mutualistic networks. The turnover of species and their interactions across landscapes is the outcome of a complex interplay between several ecological and evolutionary processes (19, 9). Our aim in these sensitivity analyses was to explore how a simple scenario of species turnover could affect our previous results. To do so, we explored the scenario in which generalist species have broad geographic ranges (9, 20). We assumed that the geographical range of each species is proportional to its degree and randomly removed species from each local network (site  $A$  and site  $B$ ) with a probability based on the degree. Before removing species, both local networks consisted of the same empirical network. In order to always maintain a core of generalist species in both local networks, we defined the probability of removing a species as  $p_i = 0$  if  $k_i \geq \bar{k}$  or  $p_i = 1 - \frac{k_i}{\bar{k}}$  if  $k_i < \bar{k}$ , where  $\bar{k}$  is the mean degree value in the network. Thus, species with degree

values greater or equal to  $\bar{k}$  always remained at both local networks and the other species were removed independently from each network according to  $p_i$ . After removing species from both networks according to this process, we simulated the coevolutionary dynamics according to equation [S7]. Our removal procedure generated three groups of species: (i) species present at site  $A$  and site  $B$  that could be affected by gene flow across sites, (ii) species present at either site  $A$  or site  $B$  that coevolved locally without the effects of gene flow, and (iii) species removed from both sites that did not participate in the coevolutionary dynamics. In these simulations, we used two combinations of mutualistic selection ( $\bar{m}_A = \bar{m}_B = 0.7$  and  $\bar{m}_A = 0.9$ ,  $\bar{m}_B = 0.1$ ), 13 values of gene flow ( $\bar{g} = 0, 0.025, 0.05, \dots, 0.25, 0.275, 0.3$ ), and a random sample of 36 empirical networks of our complete dataset (Table S1). For each combination of  $\bar{m}_A$ ,  $\bar{m}_B$ , and  $\bar{g}$  we performed 50 simulations per empirical network ( $n = 36$  networks, total = 46,800 simulations).

In our simulations, the mean fraction of species removed from each network was  $0.33 \pm 0.12$  (mean  $\pm$  sd,  $n = 93,600$ ). We found that, when we allow species composition to vary across space, gene flow has the same effects on trait matching as observed previously (Fig. S7). Although the effects of gene flow seem weaker for intimate mutualisms in these simulations, the effects of gene flow are still strong for multiple-partner mutualisms (Fig. S7).

Overall, our simulations that imposed a correlation between gene flow and species degree (see *Simulations with gene flow correlated with species degree*) and our simulations with species turnover confirm the important role of generalist species for multispecies coevolution across space. Because gene flow increases trait matching at the network level mainly because of trait changes in generalist species, we should expect gene flow to have an important role in promoting coadaptation whenever generalist species are present at multiple locations and migrate between them.

## 2.2 Analytical approximations

### 2.2.1 Single-site coevolutionary model

We used analytical approximations of the coevolutionary models (eq. [S4] and [S7]) to understand how trait patterns emerge in mutualistic networks. In this section, we present the analytical expression for the equilibrium of the single-site coevolutionary model (eq. [S4]) as originally developed by (1). To obtain this analytical expression, we assumed that the evolutionary effects  $q_{ij}^{(t)}$  are fixed over time (i.e.,  $q_{ij}^{(t)} = q_{ij}$ ). We find the equilibrium by setting  $z_i^{(t+1)} = z_i^{(t)} = z_i^*$  in equation [S4]:

$$0 = \varphi_i \left[ \sum_{j=1}^N q_{ij} (z_j^* - z_i^*) + (1 - \sum_{j=1}^N q_{ij}) (\theta_i - z_i^*) \right] \quad [\text{S15}]$$

$$z_i^* = \sum_{j=1}^N q_{ij} z_j^* + (1 - \sum_{j=1}^N q_{ij}) \theta_i \quad [\text{S16}]$$

Using the fact that  $\sum_{j=1}^N q_{ij} = m_i$ , equation [S16] can be rewritten as:

$$z_i^* = \sum_{j=1}^N q_{ij} z_j^* + (1 - m_i) \theta_i \quad [\text{S17}]$$

The above equation may be written for all the  $N$  species in the mutualistic assemblage as:

$$\mathbf{z}^* = \mathbf{Q}\mathbf{z}^* + \boldsymbol{\Psi}\boldsymbol{\theta} \quad [\text{S18}]$$

where  $\mathbf{z}^*$ ,  $\boldsymbol{\theta}$ ,  $\mathbf{Q}$ , and  $\boldsymbol{\Psi}$  are the following vectors and matrices:

$$\mathbf{z}^* = \begin{bmatrix} z_1^* \\ z_2^* \\ \vdots \\ z_N^* \end{bmatrix}, \boldsymbol{\theta} = \begin{bmatrix} \theta_1 \\ \theta_2 \\ \vdots \\ \theta_N \end{bmatrix}, \mathbf{Q} = \begin{bmatrix} q_{11} & q_{12} & \cdots & q_{1N} \\ q_{21} & q_{22} & \cdots & q_{2N} \\ \vdots & \vdots & \ddots & \vdots \\ q_{N1} & q_{N2} & \cdots & q_{NN} \end{bmatrix}, \boldsymbol{\Psi} = \begin{bmatrix} 1 - m_1 & 0 & \cdots & 0 \\ 0 & 1 - m_2 & \cdots & 0 \\ \vdots & \vdots & \ddots & \vdots \\ 0 & 0 & \cdots & 1 - m_N \end{bmatrix}$$

Equation [S18] may be further simplified, leading to the final equation in matrix form for the equilibrium of the single-site model:

$$\mathbf{z}^* = (\mathbf{I} - \mathbf{Q})^{-1} \boldsymbol{\Psi} \boldsymbol{\theta} \quad [\text{S19}]$$

where  $\mathbf{I}$  is the identity matrix of dimension  $N$ . As described in detail in (1), the coevolutionary matrix  $\mathbf{T} = (\mathbf{I} - \mathbf{Q})^{-1} \boldsymbol{\Psi}$  contains the direct and indirect effects that link the equilibrium trait value of each species ( $z_i^*$ ) to all values favored by the local environment ( $\boldsymbol{\theta}$ ). In particular, each element  $t_{ij}$  of  $\mathbf{T}$  contains all the direct and indirect effects of species  $j$  on the selection gradient shaping the trait evolution of species  $i$ . Thus, row  $i$  of  $\mathbf{T}$  defines the mutualistic adaptive landscape of species  $i$ .

### 2.2.2 Two-site coevolutionary model

We now present our analytical expression for the equilibrium of the two-site coevolutionary model. To obtain this expression we assumed that evolutionary effects at both sites are fixed over time (i.e.,  $q_{ij,A}^{(t)} = q_{ij,A}$  and  $q_{ij,B}^{(t)} = q_{ij,B}$ ) and that  $\varphi_{i,A} = \varphi_{i,B} = 1$  for every species  $i$ . Our sensitivity analyses show that setting  $\varphi_{i,A} = \varphi_{i,B} = 1$  does not change our results of how trait matching emerges in the two-site model (Fig. S2F). Although species composition ( $N_A$  and  $N_B$ ) and network structure may change across sites in our analytical approximation, we focused on the simple case in which both sites contain the same species composition and mutualistic network ( $N_A = N_B = N$ ). For site  $A$ , we find an expression for the equilibrium by setting  $z_{i,A}^{(t+1)} = z_{i,A}^{(t)} = z_{i,A}^*$  and  $z_{i,B}^{(t+1)} = z_{i,B}^{(t)} = z_{i,B}^*$  in equation [S7]:

$$z_{i,A}^* = (1 - g_i) \left[ z_{i,A}^* + \sum_{j=1}^N q_{ij,A} (z_{j,A}^* - z_{i,A}^*) + (1 - \sum_{j=1}^N q_{ij,A}) (\theta_{i,A} - z_{i,A}^*) \right] + g_i \left[ z_{i,B}^* + \sum_{j=1}^N q_{ij,B} (z_{j,B}^* - z_{i,B}^*) + (1 - \sum_{j=1}^N q_{ij,B}) (\theta_{i,B} - z_{i,B}^*) \right] \quad [\text{S20}]$$

$$z_{i,A}^* = (1 - g_i) \left[ \sum_{j=1}^N q_{ij,A} z_{j,A}^* + (1 - m_{i,A}) \theta_{i,A} \right] + g_i \left[ \sum_{j=1}^N q_{ij,B} z_{j,B}^* + (1 - m_{i,B}) \theta_{i,B} \right] \quad [\text{S21}]$$

In the equation above we also used the fact that  $\sum_{j=1}^N q_{ij,A} = m_{i,A}$  and  $\sum_{j=1}^N q_{ij,B} = m_{i,B}$ . We can now write equation [S21] using vectors and matrices to represent all species in both mutualistic assemblages:

$$\mathbf{z}^* = \mathbf{G}(\mathbf{Q}\mathbf{z}^* + \boldsymbol{\Psi}\boldsymbol{\theta}) \quad [\text{S22}]$$

where  $\mathbf{z}^*$ ,  $\boldsymbol{\theta}$ ,  $\mathbf{G}$ ,  $\mathbf{Q}$ , and  $\boldsymbol{\Psi}$  are vectors and matrices similar to the ones for the single-site model, but they are expanded to include the variables for both sites:

$$\mathbf{z}^* = \begin{bmatrix} z_{1,A}^* \\ \vdots \\ z_{N,A}^* \\ z_{1,B}^* \\ \vdots \\ z_{N,B}^* \end{bmatrix}, \boldsymbol{\theta} = \begin{bmatrix} \theta_{1,A} \\ \vdots \\ \theta_{N,A} \\ \theta_{1,B} \\ \vdots \\ \theta_{N,B} \end{bmatrix}, \mathbf{G} = \begin{bmatrix} 1-g_1 & \cdots & 0 & g_1 & \cdots & 0 \\ \vdots & \ddots & \vdots & \vdots & \ddots & \vdots \\ 0 & \cdots & 1-g_N & 0 & \cdots & g_N \\ g_1 & \cdots & 0 & 1-g_1 & \cdots & 0 \\ \vdots & \ddots & \vdots & \vdots & \ddots & \vdots \\ 0 & \cdots & g_N & 0 & \cdots & 1-g_N \end{bmatrix}$$

$$\mathbf{Q} = \begin{bmatrix} q_{11,A} & \cdots & q_{1N,A} & & & & \\ \vdots & \ddots & \vdots & 0 & & & \\ q_{N1,A} & \cdots & q_{NN,A} & & & & \\ & q_{11,B} & \cdots & q_{1N,B} & & & \\ 0 & & \vdots & \ddots & \vdots & & \\ & q_{N1,B} & \cdots & q_{NN,B} & & & \end{bmatrix}, \boldsymbol{\Psi} = \begin{bmatrix} 1-m_{1,A} & \cdots & 0 & & & & \\ \vdots & \ddots & \vdots & & & & 0 \\ 0 & \cdots & 1-m_{N,A} & & & & \\ & & & 1-m_{1,B} & \cdots & 0 & \\ & & & 0 & & \vdots & \ddots & \vdots \\ & & & & & 0 & \cdots & 1-m_{N,B} \end{bmatrix}$$

We now simplify equation [S22] further to obtain our final equilibrium expression in matrix form:

$$\mathbf{G}^{-1}\mathbf{z}^* - \mathbf{Q}\mathbf{z}^* = \boldsymbol{\Psi}\boldsymbol{\theta} \quad [\text{S23}]$$

$$\mathbf{z}^* = (\mathbf{G}^{-1} - \mathbf{Q})^{-1}\boldsymbol{\Psi}\boldsymbol{\theta} \quad [\text{S24}]$$

In the equation above, the matrix  $\mathbf{T} = (\mathbf{G}^{-1} - \mathbf{Q})^{-1}\boldsymbol{\Psi}$  now contains the matrix  $\mathbf{G}^{-1}$  instead of the identity matrix. If we assume that  $g_i$  is the same for every species  $i$  and that  $g_i \neq 0.5$  (if  $g_i = 0.5$ ,  $\mathbf{G}$  is not invertible), then  $\mathbf{G}^{-1}$  has the following structure:

$$\mathbf{G}^{-1} = \begin{bmatrix} 1 + \frac{g}{1-2g} & \cdots & 0 & -\frac{g}{1-2g} & \cdots & 0 \\ \vdots & \ddots & \vdots & \vdots & \ddots & \vdots \\ 0 & \cdots & 1 + \frac{g}{1-2g} & 0 & \cdots & -\frac{g}{1-2g} \\ -\frac{g}{1-2g} & \cdots & 0 & 1 + \frac{g}{1-2g} & \cdots & 0 \\ \vdots & \ddots & \vdots & \vdots & \ddots & \vdots \\ 0 & \cdots & -\frac{g}{1-2g} & 0 & \cdots & 1 + \frac{g}{1-2g} \end{bmatrix}$$

Therefore, if  $g = 0$ ,  $\mathbf{G}^{-1} = \mathbf{I}$  and the equilibrium expression becomes identical to the expression for the single-site model. However, if  $0 < g < 1$  ( $g \neq 0.5$ ), then  $\mathbf{G}^{-1}$  enables indirect coevolutionary effects that connect populations at site  $A$  with populations at site  $B$ . In this sense, this expanded version of  $\mathbf{T}$  provides both the local coevolutionary effects (diagonal blocks) and the geographical coevolutionary effects (off-diagonal blocks) that reshape species traits given the local level of mutualistic selection ( $\boldsymbol{\Psi}$ ) and the local environmental selective pressures ( $\boldsymbol{\theta}$ ). The element  $t_{ij}$  of  $\mathbf{T}$  contains all the direct and indirect effects of population  $j$  on the selection gradient shaping the trait evolution of population  $i$ , which may co-occur or not with population  $j$ . Therefore, row  $i$  of  $\mathbf{T}$  represents an enlarged adaptive landscape for species  $i$ , containing local and spatial coevolutionary effects. Below, we describe a property of the matrix  $\mathbf{T}$  that is associated

with the emergence of trait patterns in mutualistic assemblages.

### 2.2.3 Matrix $\mathbf{T}$ and the emergence of trait matching

Our analytical study shows that trait values at equilibrium ( $\mathbf{z}^*$ ) are connected to environmental optimum values ( $\boldsymbol{\theta}$ ) through a matrix ( $\mathbf{T}$ ) containing coevolutionary effects. In the single-site model,  $\mathbf{T}$  contains local coevolutionary effects and in the two-site model,  $\mathbf{T}$  contains coevolutionary effects within and between communities. Here we describe a property of  $\mathbf{T}$  that is related to the emergence of trait matching in both models. In the single-site model, row  $i$  of  $\mathbf{T}$  represents how all species in the network directly or indirectly affect the adaptive landscape of species  $i$ . Because the element  $z_i^*$  in  $\mathbf{z}^*$  is the result of the dot product of row  $i$  of  $\mathbf{T}$  and  $\boldsymbol{\theta}$ , two identical rows in  $\mathbf{T}$  lead to two identical trait values in  $\mathbf{z}^*$ , regardless of the values in the vector  $\boldsymbol{\theta}$ . In other words, if the mutualistic adaptive landscapes of two species are identical, their equilibrium trait values will be the same. In this sense, similar rows in the matrix  $\mathbf{T}$  should lead to similarity in equilibrium trait values (i.e., trait convergence) and, as a consequence, to trait matching between interacting species.

We developed a metric to measure the similarity among rows of  $\mathbf{T}$ . We called our metric the similarity of adaptive landscapes and calculated it as the mean correlation among all rows of  $\mathbf{T}$ . We now describe how we used our simulation results and additional empirical information on mutualistic interactions to investigate how mutualistic selection ( $m_{i,A}, m_{i,B}$ ) and gene flow ( $g_i$ ) affect the similarity of adaptive landscapes, leading to the emergence of trait matching. We first explored our results for the single-site coevolutionary model to understand the effect of  $m_i$ . To do so, we used the equilibrium trait values and parameter values of our simulations in order to build the matrices  $\mathbf{Q}$  and  $\boldsymbol{\Psi}$ , which make up the matrix  $\mathbf{T}$ . Note that we used only the mean value of mutualistic selection to build matrix  $\boldsymbol{\Psi}$  (i.e.,  $m_i = \bar{m} \forall i$ ), for simplicity. For each simulation result, we built the matrix  $\mathbf{T} = (\mathbf{I} - \mathbf{Q})^{-1}\boldsymbol{\Psi}$  and calculated the correlation among all possible pairs of rows. We then computed the mean correlation value and defined this value as the similarity of adaptive landscapes. Finally, we calculated the equilibrium trait values ( $z_i^*$ ) using the  $\theta_i$  values and our equilibrium expression (eq. [S19]). We then computed the mean equilibrium trait matching using equation [S10].

Our analyses show that higher values of mutualistic selection ( $m_i$ ) lead to a greater similarity of mutualistic adaptive landscapes in the network (Fig. S8). As shown in Fig. S8, this result is a consequence of the fact that indirect effects become stronger when mutualistic selection is higher (1). We also found that a greater similarity of adaptive landscapes is associated with higher values of trait matching in our simulations for all types of mutualism (Fig. S9).

Our next step was to analyze how gene flow ( $g_i$ ) affects the similarity of adaptive landscapes in the matrix  $\mathbf{T}$  in two hotspots ( $\bar{m}_A = \bar{m}_B = 0.7$ ) and in a hotspot and a coldspot ( $\bar{m}_A = 0.9$  and  $\bar{m}_B = 0.1$ ). As described above for the single-site model, we used the equilibrium trait values and parameter values of our simulations in order to build the matrix  $\mathbf{T} = (\mathbf{G}^{-1} - \mathbf{Q})^{-1}\boldsymbol{\Psi}$ . We used the mean values of gene flow and mutualistic selection (i.e.,  $g_i = \bar{g}$ ,  $m_{i,A} = \bar{m}_A$ ,  $m_{i,B} = \bar{m}_B \forall i$ ) to build  $\mathbf{G}$  and  $\boldsymbol{\Psi}$ , respectively. For each simulation result, we built the matrix  $\mathbf{T}$ , calculated the mean correlation among its rows, and computed the mean equilibrium trait matching for each site using our analytical expression (eq. [S24]) and trait matching formula (eq. [S10]).

We found that, with two hotspots, gene flow ( $g_i$ ) favors the similarity of mutualistic adaptive landscapes in the matrix  $\mathbf{T}$  (Fig. S10). By promoting indirect coevolutionary effects that connect species present in different sites, gene flow makes mutualistic adaptive landscapes more similar to each other (Fig. S10). As a result, gene flow favors the emergence of trait matching in our simulations with two hotspots for all types

of mutualism (Fig. S11A). However, when a hotspot is connected to a coldspot, gene flow decreases the similarity of adaptive landscapes and, as a consequence, inhibits the emergence of trait matching for all types of mutualism (Fig. S11B). Therefore, by measuring how mutualistic selection and gene flow affect an important property of the matrix  $\mathbf{T}$ , we showed how these parameters can allow trait matching to emerge by homogenizing adaptive landscapes of different species through local and spatial indirect coevolutionary effects.

### 3 Network structure and the evolution of trait patterns

Having shown that gene flow favors the emergence of trait matching in mutualistic networks, our next step was to investigate how the organization of interactions in these networks affects trait evolution. To do so, we measured four metrics of network structure and performed a Principal Component Analysis (PCA) to summarize the variation in network structure of our dataset (Table S1). Here we describe in detail how we characterized network structure and performed our PCA.

#### 3.1 Network structure metrics

Each mutualistic network in our dataset is composed of two distinct sets of species (e.g., pollinators and plants) and interactions only occur between species of different sets. To quantify structural metrics, we represented each network as a bipartite matrix  $\mathbf{B}$  containing the  $N_1$  species of the first set on the rows and the  $N_2$  species of the second set on the columns. In matrix  $\mathbf{B}$  ( $N_1 \times N_2$ ), an element  $b_{ij} = 1$  if species  $i$  and  $j$  interact as mutualistic partners or  $b_{ij} = 0$  if they do not interact. Note that the adjacency matrix  $\mathbf{A}$  used to parameterize the coevolutionary models (see *Coevolutionary models*) contains the same information as matrix  $\mathbf{B}$ , but has all species in the rows and in the columns.

Using matrix  $\mathbf{B}$ , we calculated four metrics: (i) species richness, (ii) connectance, (iii) nestedness, and (iv) modularity. Species richness was calculated as  $N = N_1 + N_2$ . Connectance represents the proportion of all possible interactions that are in fact realized (21). We calculated connectance using the following formula:

$$C = \frac{L}{N_1 N_2} \quad [S25]$$

in which  $L = \sum_{i=1}^{N_1} \sum_{j=1}^{N_2} b_{ij}$  is the total number of interactions in the network. Nestedness measures how much the interactions of species with low degree values are proper subsets of the interactions of species from the same set that have higher degree values (22). We quantified nestedness using a metric based on overlap and decreasing fill ( $NODF$ ), which varies from 0 (no nestedness) to 100 (perfect nestedness) (23, 24).  $NODF$  was computed using the following equation:

$$NODF = \frac{\sum_{i < j}^{N_1} M_{ij} + \sum_{i < j}^{N_2} M_{ij}}{\left[ \frac{N_1(N_1-1)}{2} \right] + \left[ \frac{N_2(N_2-1)}{2} \right]} \quad [S26]$$

in which the sum on the left is over all pairs of species in the first set and the sum on the right is over all pairs of species in the second set. For each pair of species  $i$  and  $j$ ,  $M_{ij}$  is defined in the following way:

$$M_{ij} = \begin{cases} \frac{n_{ij}}{\min(k_i, k_j)}, & \text{if } k_i \neq k_j \\ 0, & \text{if } k_i = k_j \end{cases} \quad [S27]$$

in which  $n_{ij}$  is the number of common interactions between  $i$  and  $j$  and  $k_i$  is the number of interactions (or degree) of species  $i$ .

Finally, modularity measures how much the network is partitioned in groups of species (i.e., modules) with many interactions within groups and few interactions among different groups (25). We quantified modularity using a bipartite version of the metric  $Q$ , which varies from 0 (no modularity) to 1 (perfect modularity) (26, 24). The bipartite version of  $Q$  has the following equation:

$$Q = \sum_{i=1}^n \left( \frac{e_i}{L} - \frac{d_i^{N_1}}{L} \frac{d_i^{N_2}}{L} \right) \quad [\text{S28}]$$

where  $n$  is the number of modules,  $e_i$  is the total number of interactions within module  $i$ , and  $d_i^{N_1}$  ( $d_i^{N_2}$ ) is the sum of the degrees of species from the first (or second) set within module  $i$ . Each partition of a network in modules renders a different value of  $Q$ . Thus, we used an optimization algorithm based on simulated annealing that numerically maximizes  $Q$  and finds the partition that best reflects the organization of the network in modules (27). Modularity was calculated using the program MODULAR (27) and the other metrics were calculated in R 3.3.2 (12). All codes are available at [www.github.com/wgar84/spatial\\_coevo\\_mutnet](http://www.github.com/wgar84/spatial_coevo_mutnet).

### 3.2 Principal Component Analysis

Because network structural metrics are often highly correlated among each other (21, 22, 28), we used Principal Component Analysis (PCA) to describe how the values of our four metrics covary across networks (29, 1). We used the correlation matrix among our four metrics in the PCA because of large differences in the scale of our metrics (Table S1). By using PCA, we were able to obtain two axes of structural variation—the first two principal components ( $PC1$  and  $PC2$ )—that describe the variation in network structure of our dataset. We decided to use only those two principal components because together they explain over 93% of the variation in our dataset (percentage of variance explained by each  $PC$ :  $PC1 = 60.94\%$ ,  $PC2 = 32.43\%$ ,  $PC3 = 4.76\%$ , and  $PC4 = 1.86\%$ ). In the main text, we reported only the strongest correlations of  $PC1$  and  $PC2$  with our network metrics. Here, we report all the correlations between  $PC1$  and  $PC2$  and our network structure metrics (Table S3). The relationship between trait matching and  $PC1$  and  $PC2$  (Fig. 3) allows us to conclude that networks with few species, low connectance, low nestedness, and high modularity favor higher values of trait matching. However, when gene flow connects two mutualistic assemblages, the effect of network structure on the emergence of trait matching is much weaker (Fig. 3).

## 4 Disruption of gene flow and its consequences for coevolution

We used our analytical equilibrium expression and additional empirical data on mutualistic interactions to understand the consequences of the disruption of gene flow to the evolution of trait patterns. Here, we explain in detail how we performed this analysis and present additional results. For this analysis, we used a sample of our complete dataset of mutualistic networks for which we had data on the interaction weights ( $n = 29$  networks, Table S1). These interaction weights represent the frequency with which two species interact at a given location and, therefore, are a proxy for how much one partner depends on the other for its survival or reproduction (24). In this sense, this information may be used to parameterize the evolutionary effect of species  $j$  on species  $i$  in our coevolutionary model ( $q_{ij}$ ). We are aware that ecological effects are not equivalent to evolutionary effects, but we decided to use this approach as a first approximation that allows

inferences from empirical data. By using empirical information, we avoided using our simulation results (i.e., equilibrium trait values) to parameterize  $q_{ij}$ , as we did in *Matrix  $\mathbf{T}$  and the emergence of trait matching*. For each of the 29 quantitative empirical networks, we simulated the progressive loss of gene flow using different scenarios of mutualistic selection ( $m_{i,A}$  and  $m_{i,B}$ ) and gene flow ( $g_i$ ).

We started our simulations by building the matrices that are needed to obtain equilibrium trait values via our analytical expression (eq. [S24]), that is,  $\mathbf{G}$ ,  $\Psi$ , and  $\mathbf{Q}$ . Matrix  $\mathbf{G}$  was initially built using a high value of gene flow, which was either  $g_i = 0.1 \forall i$  or  $g_i = 0.3 \forall i$ . Matrix  $\Psi$  was built using a given value for  $m_{i,A}$  and  $m_{i,B}$ . All species from a given site had the same value of  $m_{i,A}$  or  $m_{i,B}$ . We performed simulations using 15 different combinations of  $m_{i,A}$  and  $m_{i,B}$  (Table S2). Matrix  $\mathbf{Q}$  was built using the  $m_{i,A}$  and  $m_{i,B}$  values as well as the empirical information on interaction weights contained in our quantitative empirical networks. After building those matrices, our simulations had three additional steps. First, we computed equilibrium trait values ( $\mathbf{z}^*$ ) using equation [S24] for 10 different samples of  $\theta$  with  $\theta_{i,A} \sim \mathcal{U}[0, 10]$  and  $\theta_{i,B} \sim \mathcal{U}[10, 20]$ . Second, we quantified the mean equilibrium trait matching ( $\bar{\tau}^*$ ) within each site using equation [S10] for each of our 10 samples of  $\theta$ . Third, we perturbed  $\mathbf{G}$  by randomly choosing 5% of the species in the network and changing their gene flow value from high to low, which was either  $g_i = 0.05$ ,  $g_i = 0.01$ , or  $g_i = 0$ . By doing so, we altered the direct and indirect coevolutionary effects present in the matrix  $\mathbf{T} = (\mathbf{G}^{-1} - \mathbf{Q})^{-1}\Psi$ . After perturbing the matrix  $\mathbf{G}$ , we repeated these three steps until all species in the network had a low value of gene flow, which was the end of the simulation. For each network and each parameter choice (i.e., each combination of  $m_{i,A}$ ,  $m_{i,B}$ , high  $g_i$ , and low  $g_i$ ;  $n = 105$  combinations), we performed 10 simulations in order to vary the sequence of species that lost gene flow ( $n = 29$  networks, total = 30,450 simulations). All codes are available at [www.github.com/wgar84/spatial\\_coevo\\_mutnet](https://www.github.com/wgar84/spatial_coevo_mutnet).

Our results for high  $g_i = 0.3$  and low  $g_i = 0$  show that disruption of gene flow causes trait matching to initially decrease in mutualistic networks (Fig. S12). However, we found that extreme loss of gene flow may cause trait matching to increase (Fig. S12). For some specific combinations of mutualistic selection, such as a hotspot and a coldspot ( $m_{i,A} = 0.9$ ,  $m_{i,B} = 0.1$ ), trait matching values in the absence of gene flow ( $g_i = 0$ ) are higher than initial trait matching values ( $g_i = 0.3$ ). Thus, our results suggest that the effect of gene flow on trait matching depends not only on the levels of mutualistic selection, but also on the fraction of species with a high value of gene flow.

We also found that, for  $m_{i,A} = 0.5$  and  $m_{i,B} = 0.5$ , the choice of the high and low values of gene flow do not qualitatively affect our conclusion that losing gene flow causes trait matching to decrease (Fig. S13). These different parameterizations for high and low gene flow also allowed us to explore how the variation in gene flow across species in the network affects the emergence of trait matching. To do so, we calculated the standard deviation of  $g_i$  values throughout the simulations. Our results show that a larger variation of gene flow values leads to a stronger decrease in trait matching as gene flow is lost (Fig. S13). Furthermore, our results suggest that the slight increase in trait matching in the end of the simulations is associated with a decrease in the variation of gene flow values (Fig. S13). Therefore, variation in dispersal ability and gene flow across species should play an important role in trait evolution in mutualistic assemblages.

## References

- (1) Guimarães PR, Pires MM, Jordano P, Bascompte J, Thompson JN (2017) Indirect effects drive coevolution in mutualistic networks. *Nature* 550(7677):511–514.

- (2) Nuismer SL, Gomulkiewicz R, Ridenshour BJ (2010) When Is Correlation Coevolution? *Am Nat* 175(5):525–537.
- (3) Nuismer SL, Jordano P, Bascompte J (2013) Coevolution and the architecture of mutualistic networks. *Evolution* 67(2):338–354.
- (4) Lande R (1976) Natural selection and random genetic drift in phenotypic evolution. *Evolution* 30(2):314–334.
- (5) Santamaría L, Rodríguez-Gironés MA (2007) Linkage Rules for Plant–Pollinator Networks: Trait Complementarity or Exploitation Barriers? *PLoS Biol* 5(2):0354–0362.
- (6) Andreazzi CS, Thompson JN, Guimarães Jr PR (2017) Network Structure and Selection Asymmetry Drive Coevolution in Species-Rich Antagonistic Interactions. *Am Nat* 190(1):99–115.
- (7) Jordano P, Bascompte J, Olesen JM (2003) Invariant Properties in Coevolutionary Networks of Plant–Animal Interactions. *Ecol Lett* 6(1):69–81.
- (8) Pilosof S, Porter MA, Pascual M, Kéfi S (2017) The multilayer nature of ecological networks. *Nat Ecol Evol* 1(4):1–9.
- (9) Emer C, et al. (2018) Seed-dispersal interactions in fragmented landscapes – a metanetwork approach. *Ecol Lett* 21(4):484–493.
- (10) Carstensen DW, Sabatino M, Trøjelsgaard K, Morellato LPC (2014) Beta diversity of plant-pollinator networks and the spatial turnover of pairwise interactions. *PLoS One* 9(11):1–7.
- (11) Trojelsgaard K, Jordano P, Carstensen DW, Olesen JM (2015) Geographical variation in mutualistic networks: similarity, turnover and partner fidelity. *Proc Biol Sci* 282(1802):20142925.
- (12) R Core Team (2016) R: A language and environment for statistical computing.
- (13) Guimarães PR, Jordano P, Thompson JN (2011) Evolution and coevolution in mutualistic networks. *Ecol Lett* 14(9):877–885.
- (14) Thompson JN (2005) *The geographic mosaic of coevolution*. (The University of Chicago Press, Chicago, Illinois).
- (15) Anderson B, Johnson SD (2008) The Geographical Mosaic of Coevolution in a Plant-Pollinator Mutualism. *Evolution* 62(1):220–225.
- (16) Gómez JM, Perfectti F, Bosch J, Camacho JPM (2009) A geographic selection mosaic in a generalized plant-pollinator-herbivore system. *Ecol Monogr* 79(2):245–263.
- (17) Galetti M, et al. (2013) Functional Extinction of Birds Drives Rapid Evolutionary Changes in Seed Size. *Science* 340(6136):1086–1090.
- (18) Fort H, Vázquez DP, Lan BL (2016) Abundance and generalisation in mutualistic networks: Solving the chicken-and-egg dilemma. *Ecol Lett* 19(1):4–11.
- (19) Urban MC, et al. (2008) The evolutionary ecology of metacommunities. *Trends Ecol Evol* 23(6):311–317.

- (20) Biesmeijer JC, et al. (2006) Parallel Declines in Pollinators and Insect-Pollinated Plants in Britain and the Netherlands. *Science* 313(5785):351–354.
- (21) Jordano P (1987) Patterns of mutualistic interactions in pollination and seed dispersal: connectance, dependence asymmetries, and coevolution. *Am Nat* 129(5):657–677.
- (22) Bascompte J, Jordano P, Melián CJ, Olesen JM (2003) The nested assembly of plant–animal mutualistic networks. *Proc Natl Acad Sci USA* 100(16):9383–9387.
- (23) Almeida-Neto M, Guimarães P, Guimarães PR, Loyola RD, Ulrich W (2008) A consistent metric for nestedness analysis in ecological systems: reconciling concept and measurement. *Oikos* 117(8):1227–1239.
- (24) Bascompte J, Jordano P (2014) *Mutualistic Networks*. (Princeton University Press, Princeton, New Jersey).
- (25) Olesen JM, Bascompte J, Dupont YL, Jordano P (2007) The modularity of pollination networks. *Proc Natl Acad Sci USA* 104(50):19891–19896.
- (26) Barber MJ (2007) Modularity and community detection in bipartite networks. *Phys Rev E* 76(6):066102.
- (27) Marquitti FMD, Guimarães PR, Pires MM, Bittencourt LF (2014) MODULAR: Software for the Autonomous Computation of Modularity in Large Network Sets. *Ecography* 37(3):221–224.
- (28) Fortuna MA, et al. (2010) Nestedness versus modularity in ecological networks: two sides of the same coin? *J Anim Ecol* 79(4):811–817.
- (29) Sazima C, Guimarães PR, dos Reis SF, Sazima I (2010) What makes a species central in a cleaning mutualism network? *Oikos* 119(8):1319–1325.
- (30) Ricciardi F, Boyer M, Ollerton J (2010) Assemblage and interaction structure of the anemonefish-anemone mutualism across the Manado region of Sulawesi, Indonesia. *Environ Biol Fishes* 87(4):333–347.
- (31) Davidson DW, Snelling RR, Longino JT (1989) Competition Among Ants for Myrmecophytes and the Significance of Plant Trichomes. *Biotropica* 21(1):64–73.
- (32) Fonseca CR, Ganade G (1996) Asymmetries, compartments and null interactions in an Amazonian ant-plant community. *J Anim Ecol* 65(3):339–347.
- (33) Guimarães PR, et al. (2007) Interaction Intimacy Affects Structure and Coevolutionary Dynamics in Mutualistic Networks. *Curr Biol* 17(20):1797–1803.
- (34) Blüthgen N, Stork NE, Fiedler K (2004) Bottom-up control and co-occurrence in complex communities: Honeydew and nectar determine a rainforest ant mosaic. *Oikos* 106(2):344–358.
- (35) Guimarães PR, Rico-Gray V, dos Reis SF, Thompson JN (2006) Asymmetries in specialization in ant-plant mutualistic networks. *Proc Biol Sci* 273(1597):2041–2047.
- (36) Johnson WS, Ruben P (1988) Cleaning behavior of Bodianus rufus, Thalassoma bifasciatum, Gobiosoma evelynae, and Periclimenes pedersoni along a depth gradient at Salt River Submarine Canyon, St. Croix. *Environ Biol Fishes* 23(3):225–232.

- (37) Guimarães PR, Sazima C, dos Reis SF, Sazima I (2007) The nested structure of marine cleaning symbiosis: is it like flowers and bees? *Biol Lett* 3(1):51–54.
- (38) Wicksten MK (1998) Behaviour of cleaners and their client fishes at Bonaire, Netherlands Antilles. *J Nat Hist* 32(1):13–30.
- (39) Arroyo MTK, Primack R, Armesto J (1982) Community Studies in Pollination Ecology in the High Temperate Andes of Central Chile. I. Pollination Mechanisms and Altitudinal Variation. *Am J Bot* 69(1):82–97.
- (40) Barrett SCH, Hellenurm K (1987) The reproductive biology of boreal forest herbs. I. Breeding systems and pollination. *Can J Bot* 65(10):2036–2046.
- (41) Bezerra ELS, MacHado IC, Mello MAR (2009) Pollination networks of oil-flowers: A tiny world within the smallest of all worlds. *J Anim Ecol* 78(5):1096–1101.
- (42) Dicks LV, Corbet Sa, Pywell RF (2002) Compartmentalization in plant–insect flower visitor webs. *J Anim Ecol* 71(1):32–43.
- (43) Dupont YL, Hansen DM, Olesen JM (2003) Structure of a plant–flower–visitor network in the high-altitude sub-alpine desert of Tenerife, Canary Islands. *Ecography* 26(3):301–310.
- (44) Elberling H, Olesen J (1999) The structure of a high latitude plant-flower visitor system: the dominance of flies. *Ecography* 22(3):314–323.
- (45) Hocking B (1968) Insect-Flower Associations in the High Arctic with Special Reference to Nectar. *Oikos* 19(2):359–387.
- (46) Inouye DW, Pyke GH (1988) Pollination biology in the Snowy Mountains of Australia: Comparisons with montane Colorado, USA. *Austral Ecol* 13(2):191–210.
- (47) Kaiser-Bunbury CN, Memmott J, Müller CB (2009) Community structure of pollination webs of Mauritian heathland habitats. *Perspect Plant Ecol Syst* 11(4):241–254.
- (48) Medan D, et al. (2002) Plant-Pollinator Relationships at Two Altitudes in the Andes of Mendoza, Argentina. *Arct Antarct Alp Res* 34(3):233–241.
- (49) Mosquin T, Martin JE (1967) Observations on the pollination biology of plants on Melville Island, N.W.T., Canada. *The Canadian Field-Naturalist* 81:201–205.
- (50) Olesen JM, Eskildsen LI, Venkatasamy S (2002) Invasion of pollination networks on oceanic islands: Importance of invader complexes and endemic super generalists. *Divers Distrib* 8(3):181–192.
- (51) Ollerton J, Johnson SD, Cranmer L, Kellie S (2003) The pollination ecology of an assemblage of grassland asclepiads in South Africa. *Ann Bot* 92(6):807–834.
- (52) Primack RB (1983) Insect pollination in the New Zealand mountain flora. *NZ J Bot* 21(3):317–333.
- (53) Ramirez N, Brito Y (1992) Pollination biology in a palm swamp community in the Venezuelan Central Plains. *Bot J Linn Soc* 110(4):277–302.

- (54) Santos GMdM, Aguiar CML, Mello MA (2010) Flower-visiting guild associated with the Caatinga flora: trophic interaction networks formed by social bees and social wasps with plants. *Apidologie* 41(4):466–475.
- (55) Schemske DW, et al. (1978) Flowering Ecology of Some Spring Woodland Herbs. *Ecology* 59(2):351–366.
- (56) Small E (1976) Insect pollinators of the Mer Bleue peat bog of Ottawa. *The Canadian Field-Naturalist* 90:22–28.
- (57) Vázquez DP, Simberloff D (2002) Ecological Specialization and Susceptibility to Disturbance: Conjectures and Refutations. *Am Nat* 159(6):606–623.
- (58) Baird JW (1980) The Selection and Use of Fruit by Birds in an Eastern Forest. *Wilson Bull* 92(1):63–73.
- (59) Beehler B (1983) Frugivory and Polygamy in Birds of Paradise. *The Auk* 100(1):1–12.
- (60) Carlo T, Collazo J, Groom M (2003) Avian fruit preferences across a Puerto Rican forested landscape: pattern consistency and implications for seed removal. *Oecologia* 134(1):119–131.
- (61) Crome FH (1975) The ecology of fruit pigeons in tropical Northern Queensland. *Wildlife Research* 2(2):155–185.
- (62) Donatti CI, et al. (2011) Analysis of a hyper-diverse seed dispersal network: modularity and underlying mechanisms. *Ecol Lett* 14(8):773–781.
- (63) Galetti M, Pizo M (1996) Fruit eating birds in a forest fragment in southeastern Brazil. *Ararajuba* 4:71–79.
- (64) Jordano P (1985) El ciclo anual de los paseriformes frugívoros en el matorral mediterráneo del sur de España: importancia de su invernada y variaciones interanuales. *Ardeola* 32(1):69–94.
- (65) Kantak GE (1979) Observations on Some Fruit-Eating Birds in Mexico. *The Auk* 96(1):183–186.
- (66) Lambert F (1989) Fig-Eating by Birds in a Malaysian Lowland Rain Forest. *J Trop Ecol* 5(4):401–412.
- (67) Mack AL, Wright DD (1996) Notes on Occurrence and Feeding of Birds at Crater Mountain Biological Research Station, Papua New Guinea. *Emu* 96(2):89–101.
- (68) Poulin B, Wright SJ, Lefebvre G, Calderón O (1999) Interspecific synchrony and asynchrony in the fruiting phenologies of congeneric bird-dispersed plants in Panama. *J Trop Ecol* 15(2):213–227.
- (69) Schleuning M, et al. (2011) Specialization and interaction strength in a tropical plant-frugivore network differ among forest strata. *Ecology* 92(1):26–36.
- (70) Sorenson AE (1981) Interactions between birds and fruit in a temperate woodland. *Oecologia* 50(2):242–249.

## **5 Figures and tables**

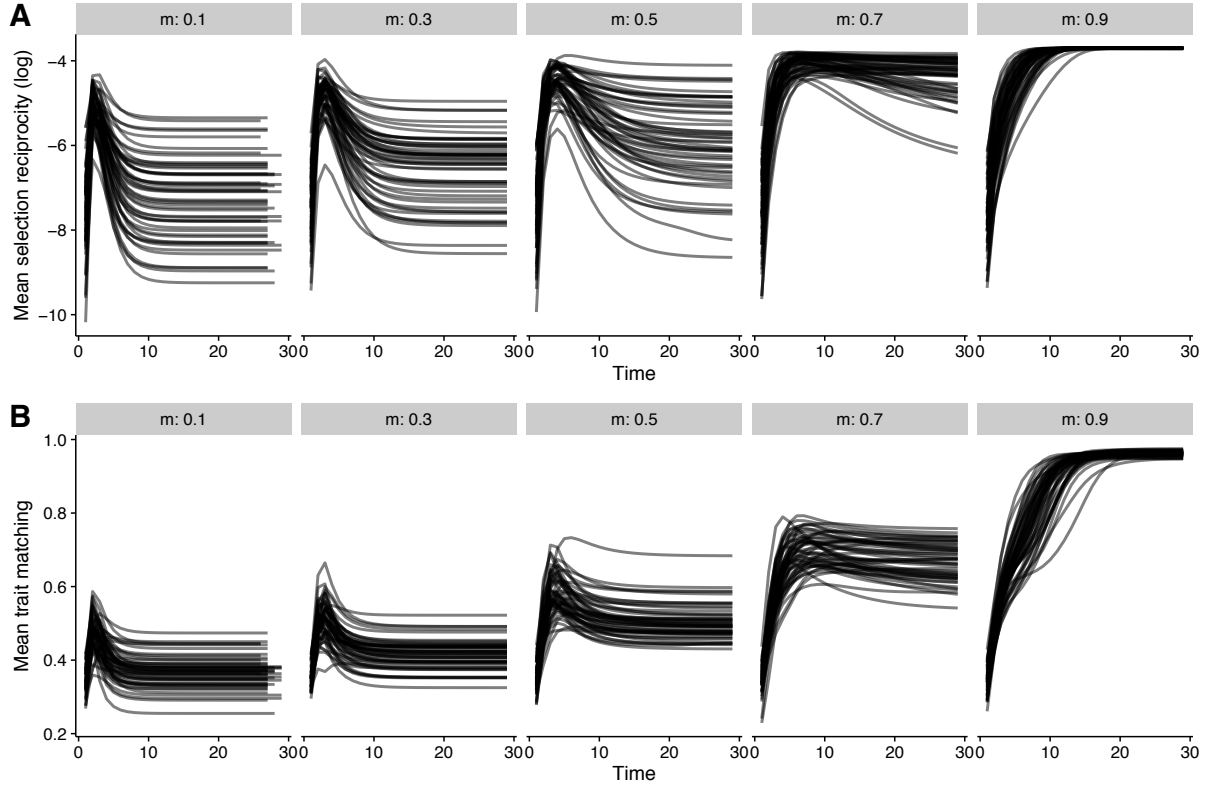


Figure S1: Higher values of mean mutualistic selection ( $\bar{m}$ ) lead to (A) stronger reciprocal selection and to (B) higher trait matching values. Each line represents the value of (A) mean reciprocity of selection ( $\log(\bar{r}^{(t)})$ ) or (B) mean trait matching ( $\bar{r}^{(t)}$ ) through time for one simulation of the single-site coevolutionary model parameterized by one empirical network (network 64 in Table S1). Each panel shows simulations for the indicated value of mean mutualistic selection ( $\bar{m}$ ). Results are shown for the first 30 timesteps to facilitate visualization, although some simulations lasted much longer. Sample distributions and values for simulation parameters:  $\varphi_i \sim \mathcal{N}[\mu = 0.5, \sigma^2 = 10^{-4}]$ ,  $\theta_i \sim \mathcal{U}[a = 0, b = 10]$ ,  $m_i \sim \mathcal{N}[\bar{m}, 10^{-4}]$ , and  $\alpha = 0.2$ .

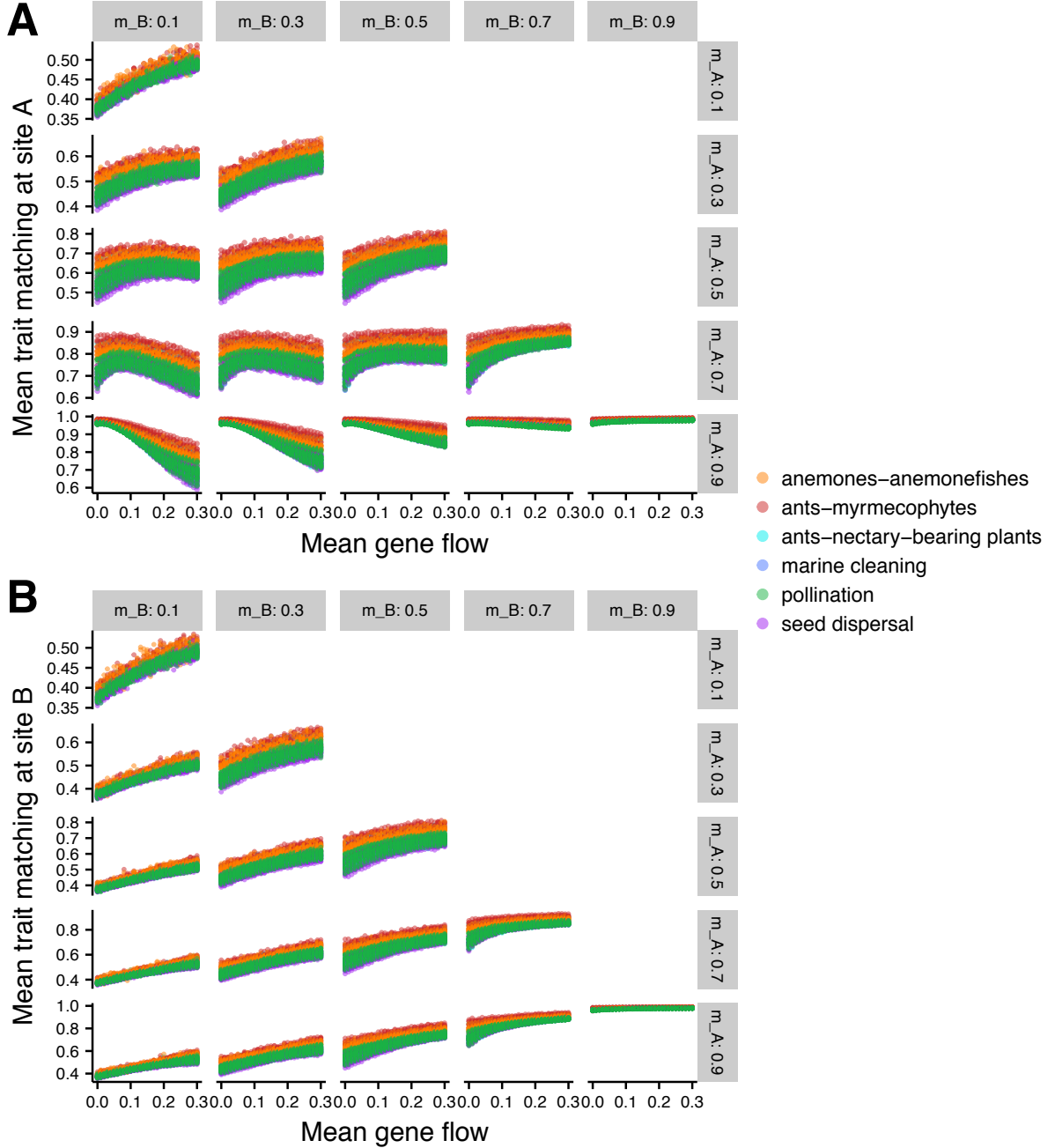


Figure S2: Gene flow favors local trait matching for the majority of combinations of mutualistic selection ( $\bar{m}_A$  and  $\bar{m}_B$ ). Each panel shows the mean trait matching at equilibrium ( $\bar{\tau}^*$ ) for different values of gene flow ( $\bar{g}$ ) for the indicated combination of mutualistic selection ( $\bar{m}_A$ : rows,  $\bar{m}_B$ : columns). (A and B) Each point is the mean of 100 simulations for a given empirical mutualistic network (total = 72 networks). Different colors represent distinct mutualisms. (A) Trait matching at site A. (B) Trait matching at site B. Sample distributions and values for simulation parameters:  $\varphi_{i,A}, \varphi_{i,B} \sim \mathcal{N}[\mu = 0.5, \sigma^2 = 10^{-4}]$ ,  $\theta_{i,A} \sim \mathcal{U}[0, 10]$ ,  $\theta_{i,B} \sim \mathcal{U}[10, 20]$ ,  $m_{i,A} \sim \mathcal{N}[\bar{m}_A, 10^{-4}]$ ,  $m_{i,B} \sim \mathcal{N}[\bar{m}_B, 10^{-4}]$ ,  $g_i \sim \mathcal{N}[\bar{g}, 10^{-6}]$ , and  $\alpha = 0.2$ .

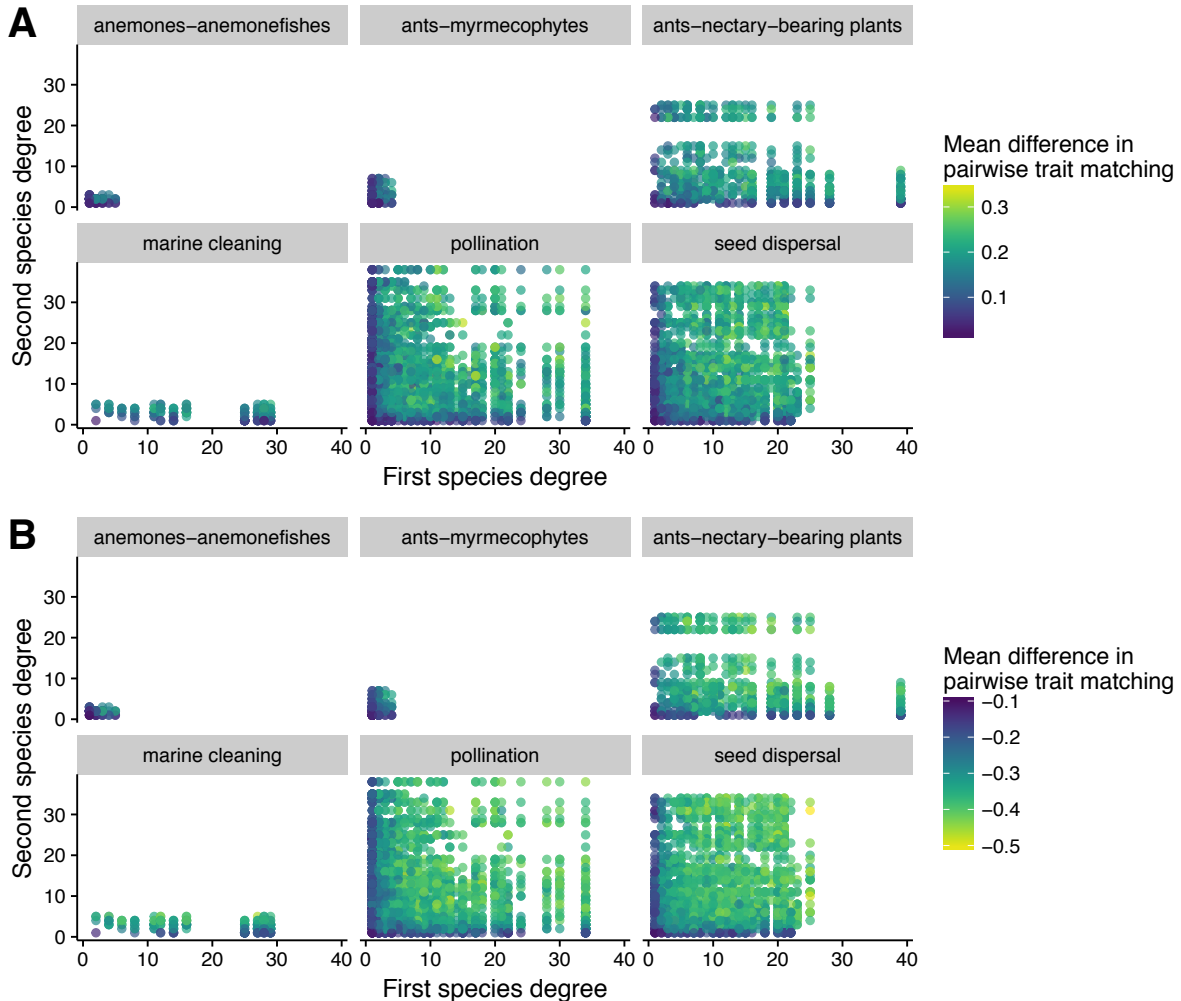


Figure S3: Gene flow fuels trait matching especially in pairs of generalist species (i.e., species with many interactions). (A and B) Each panel shows the mean difference in pairwise trait matching for simulations with and without gene flow ( $\bar{\tau}_{ij,g=0.3}^* - \bar{\tau}_{ij,g=0}^*$ ) parameterized with empirical networks of the indicated mutualism type ( $n = 72$  networks). Each point indicates the degree values ( $k_i$ ) of two interacting species (x and y axes) and the mean difference in pairwise trait matching with and without gene flow for 100 simulations (warmer colors depict higher differences in absolute value). Species with degrees larger than 40 were removed to facilitate visualization. (A) Trait matching calculated for a hotspot (site A) connected to another hotspot ( $\bar{m}_A = \bar{m}_B = 0.7$ ). (B) Trait matching calculated for a hotspot (site A) connected to a coldspot ( $\bar{m}_A = 0.9$ ,  $\bar{m}_B = 0.1$ ). Simulation parameters as in Fig. S2.

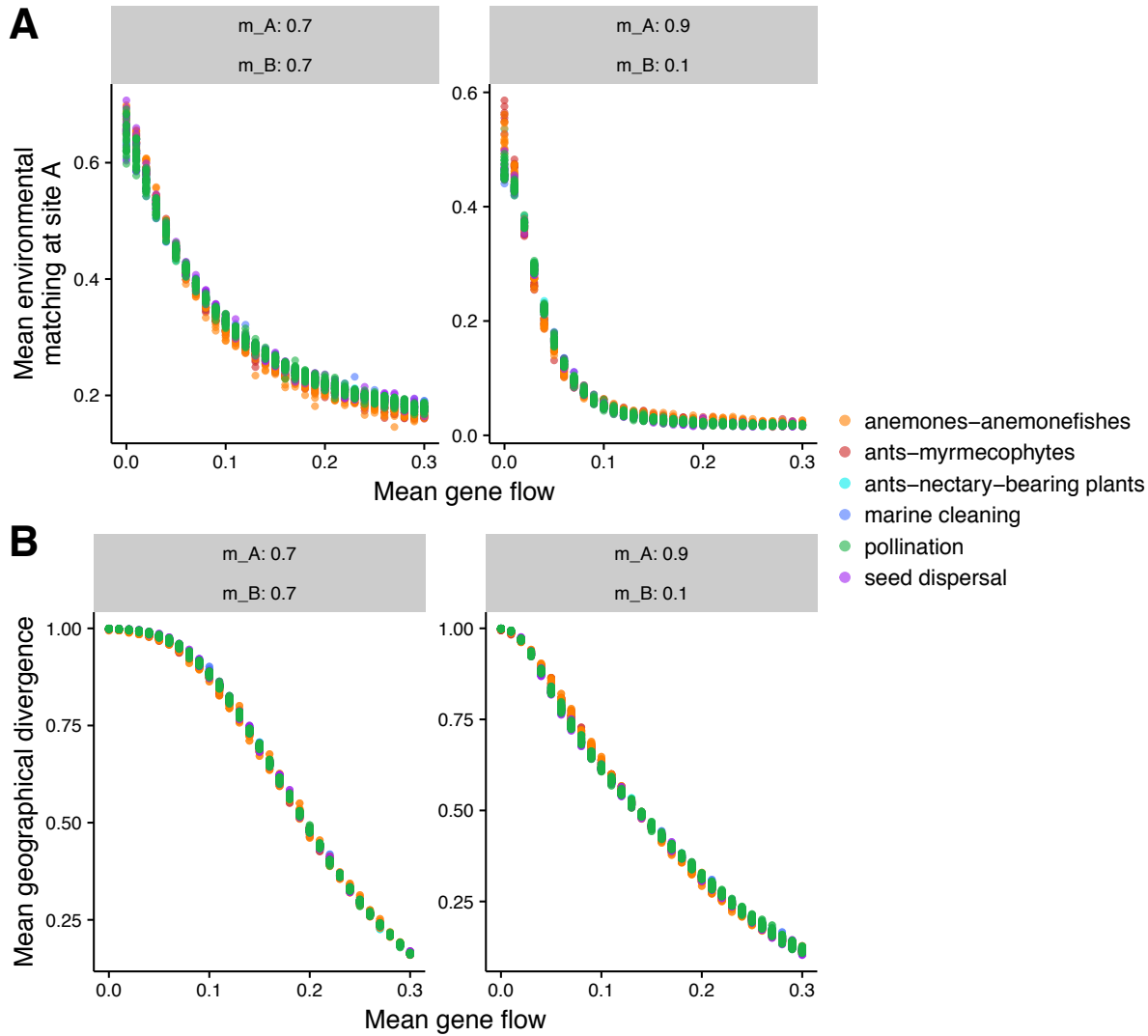


Figure S4: Gene flow promotes the uncoupling of species traits from their local environmental optima and the geographical homogenization of species traits. Panels contain the equilibrium values of (A) the mean environmental matching at site  $A$  ( $\bar{\varepsilon}_A^*$ ) or (B) the mean geographical divergence ( $\bar{\gamma}^*$ ) for different values of gene flow ( $\bar{g}$ ) and for the indicated combination of mutualistic selection ( $\bar{m}_A$  and  $\bar{m}_B$ ). Each point represents the mean of 100 simulations for a given empirical mutualistic network (total = 72 networks). Different colors represent distinct mutualisms. Simulation parameters as in Fig. S2.

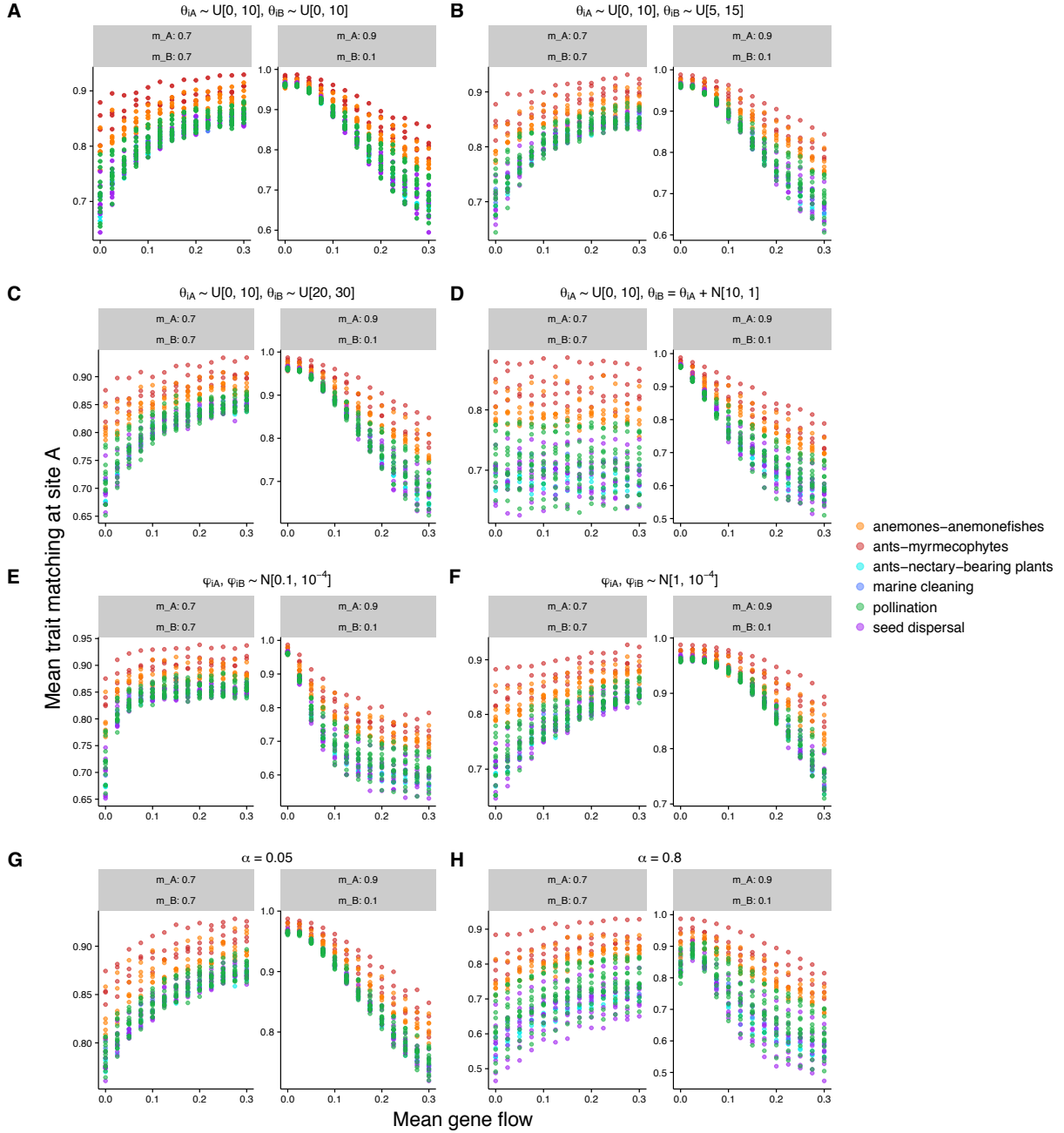


Figure S5: Gene flow enhances trait matching in a hotspot connected to another hotspot ( $\bar{m}_A = \bar{m}_B = 0.7$ ), but reduces trait matching in a hotspot connected to a coldspot ( $\bar{m}_A = 0.9, \bar{m}_B = 0.1$ ) for several different parameterizations of the two-site coevolutionary model. However, gene flow does not favor trait matching when environmental optima ( $\theta_{i,A}, \theta_{i,B}$ ) are correlated across sites (D). Each panel shows the mean trait matching at site A at equilibrium ( $\tau_A^*$ ) for different values of gene flow ( $\bar{g}$ ) and for the indicated combination of mutualistic selection ( $\bar{m}_A$  and  $\bar{m}_B$ ) and parameterization (see *Simulations with different parameterizations*). Each point represents the mean of 50 simulations for a given empirical mutualistic network (total = 36 networks). Different colors represent distinct mutualisms. (A-D) Different parameterizations of  $\theta_{i,A}$  and  $\theta_{i,B}$ , which are the trait values selected by the local environment. (E and F) Different parameterizations of  $\varphi_{i,A}$  and  $\varphi_{i,B}$ , which are related to the additive genetic variance of the trait and to the slope of the selection gradient. (G and H) Different parameterizations of  $\alpha$ , which measures the sensitivity of trait matching to differences between traits of mutualistic partners. Simulation parameters as in Fig. S2, except were noted.

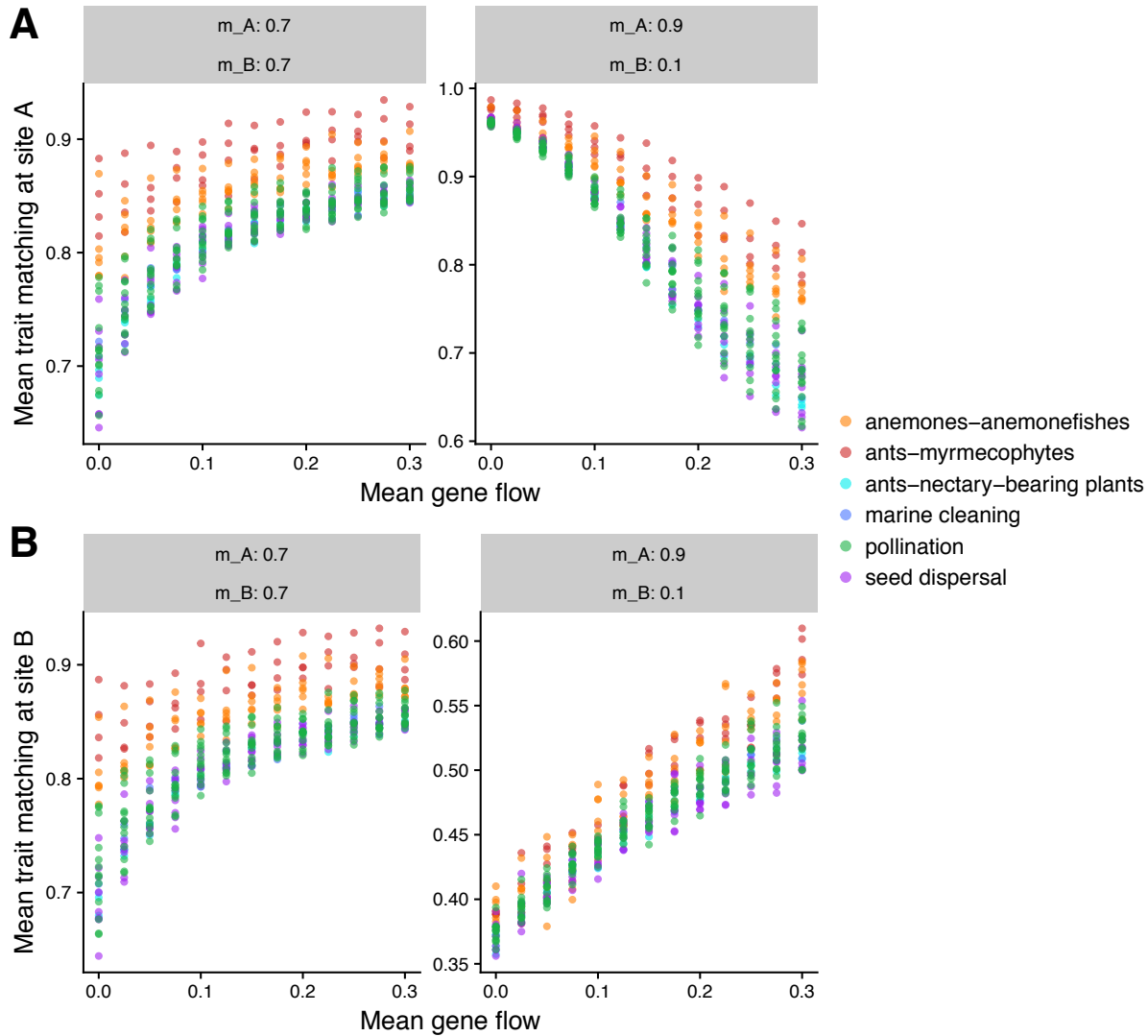


Figure S6: Gene flow enhances trait matching in a hotspot connected to another hotspot ( $\bar{m}_A = \bar{m}_B = 0.7$ ), but reduces trait matching in a hotspot connected to a coldspot ( $\bar{m}_A = 0.9$ ,  $\bar{m}_B = 0.1$ ) in simulations of the coevolutionary model in which gene flow ( $g_i$ ) is positively correlated with species degree ( $k_i$ ) (see *Simulations with gene flow correlated with species degree*). (A) Trait matching at site A. (B) Trait matching at site B. (A and B) Each point represents the mean of 50 simulations for a given empirical mutualistic network (total = 36 networks). Different colors represent distinct mutualisms. Simulation parameters as in Fig. S2, except for gene flow, which had a larger variance ( $g_i \sim \mathcal{N}[\bar{g}, 10^{-4}]$ ).

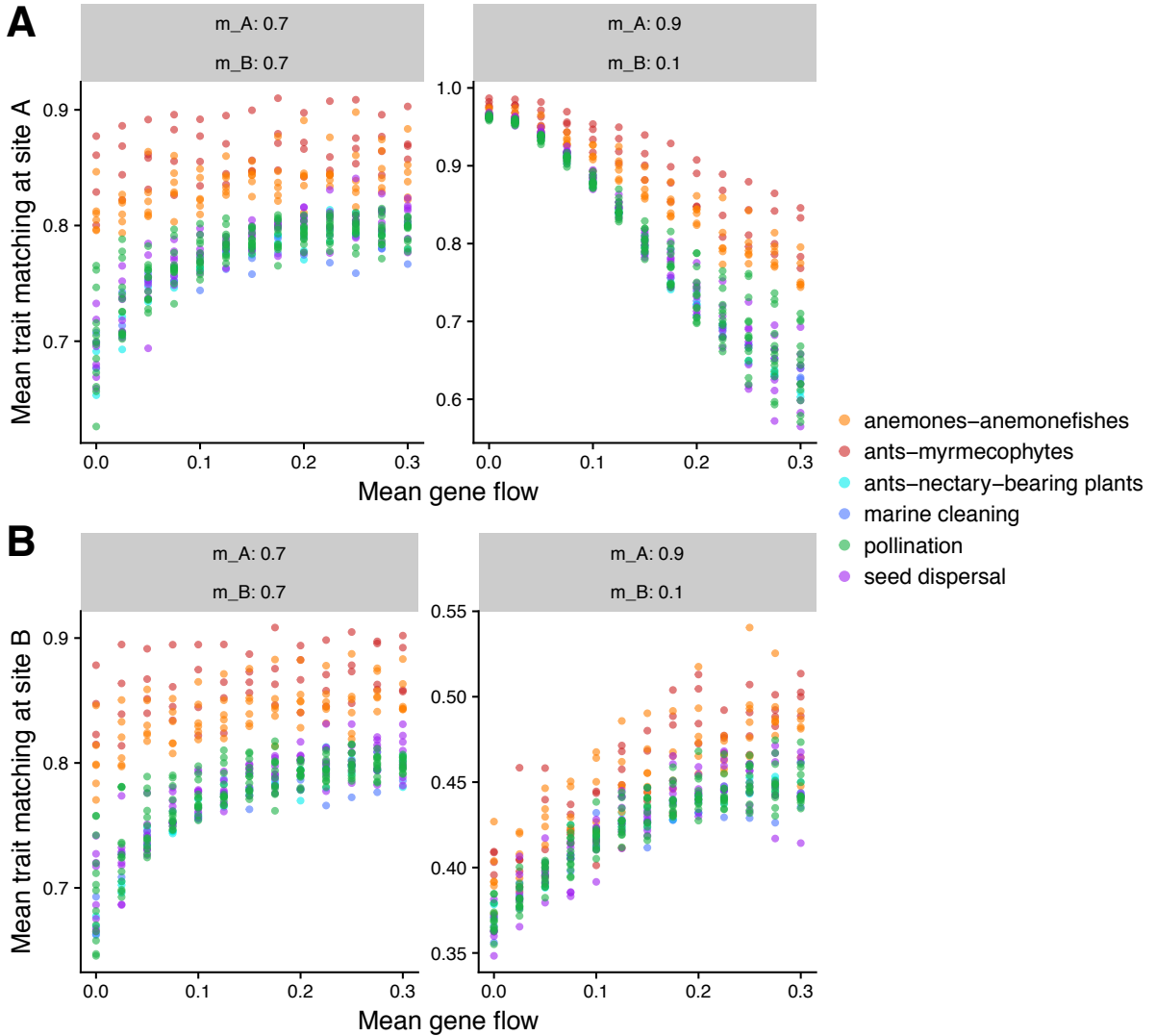


Figure S7: Gene flow enhances trait matching in a hotspot connected to another hotspot ( $\bar{m}_A = \bar{m}_B = 0.7$ ), but reduces trait matching in a hotspot connected to a coldspot ( $\bar{m}_A = 0.9$ ,  $\bar{m}_B = 0.1$ ) in simulations of the coevolutionary model with spatial species turnover. Before simulating the coevolutionary dynamics, species were randomly removed from each local mutualistic network with a probability based on species degree (see *Simulations with spatial species turnover*). (A) Trait matching at site A. (B) Trait matching at site B. (A and B) Each point represents the mean of 50 simulations for a given empirical mutualistic network (total = 36 networks). Different colors represent distinct mutualisms. Simulation parameters as in Fig. S2.

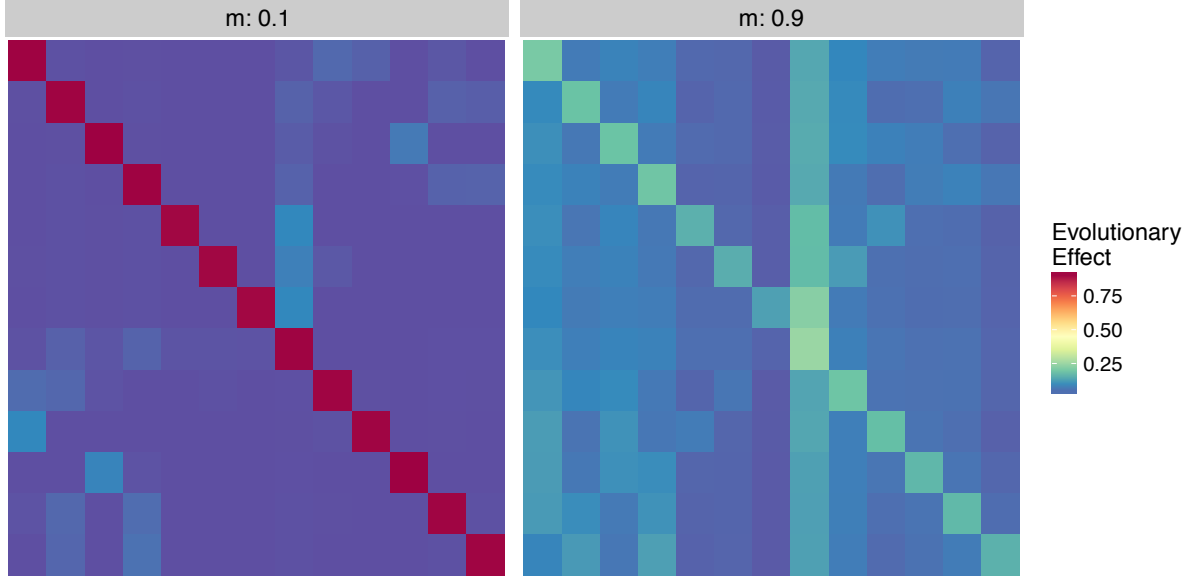


Figure S8: Higher values of mutualistic selection ( $m_i$ ) lead to greater similarity of adaptive landscapes (i.e., greater correlation among rows of matrix  $\mathbf{T}$ ). Each panel shows an example of a matrix  $\mathbf{T}$  for a seed dispersal network (network 72 in Table S1) for the indicated value of mutualistic selection (colors depict the magnitude of matrix elements). Each matrix was built using the analytical expression for the single-site coevolutionary model:  $\mathbf{T} = (\mathbf{I} - \mathbf{Q})^{-1} \Psi$ . Each matrix  $\Psi$  was built using  $m_i = 0.1 \forall i$  (left) or  $m_i = 0.9 \forall i$  (right). Each matrix  $\mathbf{Q}$  was built using equilibrium trait values ( $z_i^*$ ) and  $m_i$  values from one simulation. Sample distributions and values for simulation parameters:  $\varphi_i \sim \mathcal{N}[\mu = 0.5, \sigma^2 = 10^{-4}]$ ,  $\theta_i \sim \mathcal{U}[a = 0, b = 10]$ ,  $\alpha = 0.2$ , and  $m_i \sim \mathcal{N}[\bar{m}, 10^{-4}]$ , where  $\bar{m} = 0.1$  (left) or  $\bar{m} = 0.9$  (right).

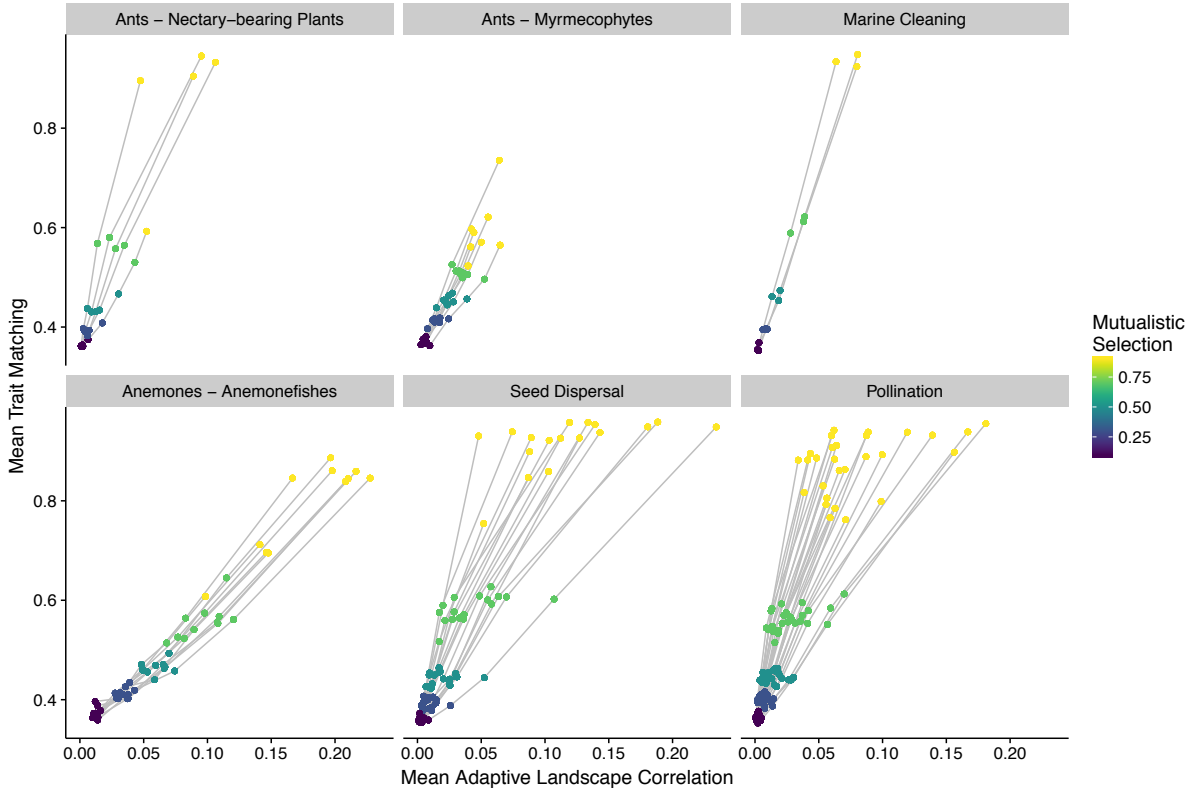


Figure S9: Greater similarity of adaptive landscapes (i.e., greater correlation among rows of matrix  $\mathbf{T}$ ) lead to higher values of trait matching. Each panel shows the mean trait matching at equilibrium ( $\bar{\tau}^*$ ) as a function of the mean correlation among mutualistic adaptive landscapes for different values of mutualistic selection ( $m_i$ , warmer colors depict higher  $m_i$  values) and for the indicated mutualism type. Trait matching and correlation among adaptive landscapes were calculated using our analytical equilibrium expression (eq. [S19]) and simulation results for the single-site coevolutionary model (see *Matrix  $\mathbf{T}$  and the emergence of trait matching*). Each point corresponds to the mean value of 100 simulations and lines connect points from the same empirical mutualistic network ( $n = 72$  networks). Simulation parameters as in Fig. S1.

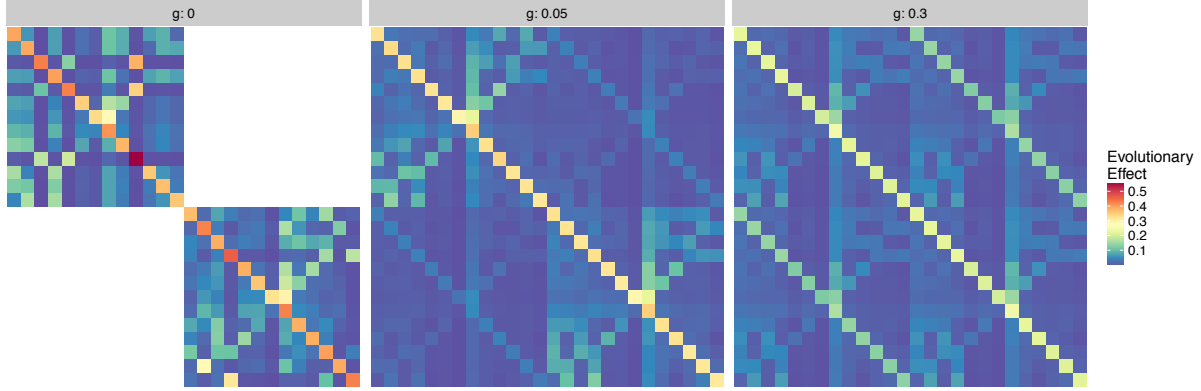


Figure S10: Higher values of gene flow ( $g_i$ ) lead to greater similarity of adaptive landscapes (i.e., greater correlation among rows of matrix  $\mathbf{T}$ ). Each panel shows an example of a matrix  $\mathbf{T}$  for a seed dispersal network (network 72 in Table S1) for the indicated value of gene flow (colors depict the magnitude of matrix elements). Each matrix was built using the analytical expression for the two-site coevolutionary model:  $\mathbf{T} = (\mathbf{G}^{-1} - \mathbf{Q})^{-1} \Psi$ . Each matrix  $\Psi$  was built using  $m_{i,A} = m_{i,B} = 0.7 \forall i$ . Each matrix  $\mathbf{G}$  was built using  $g_i = 0 \forall i$  (left),  $g_i = 0.05 \forall i$  (middle), or  $g_i = 0.3 \forall i$  (right). Each matrix  $\mathbf{Q}$  was built using equilibrium trait values ( $z_{i,A}^*$  and  $z_{i,B}^*$ ),  $m_{i,A}$  values, and  $m_{i,B}$  values from one simulation. Sample distributions and values for simulation parameters:  $\varphi_{i,A}, \varphi_{i,B} \sim \mathcal{N}[\mu = 0.5, \sigma^2 = 10^{-4}]$ ,  $\theta_{i,A} \sim \mathcal{U}[0, 10]$ ,  $\theta_{i,B} \sim \mathcal{U}[10, 20]$ ,  $\alpha = 0.2$ ,  $m_{i,A} \sim \mathcal{N}[0.7, 10^{-4}]$ ,  $m_{i,B} \sim \mathcal{N}[0.7, 10^{-4}]$ , and  $g_i \sim \mathcal{N}[\bar{g}, 10^{-6}]$ , where  $\bar{g} = 0$  (left),  $\bar{g} = 0.05$  (middle), or  $\bar{g} = 0.3$  (right).

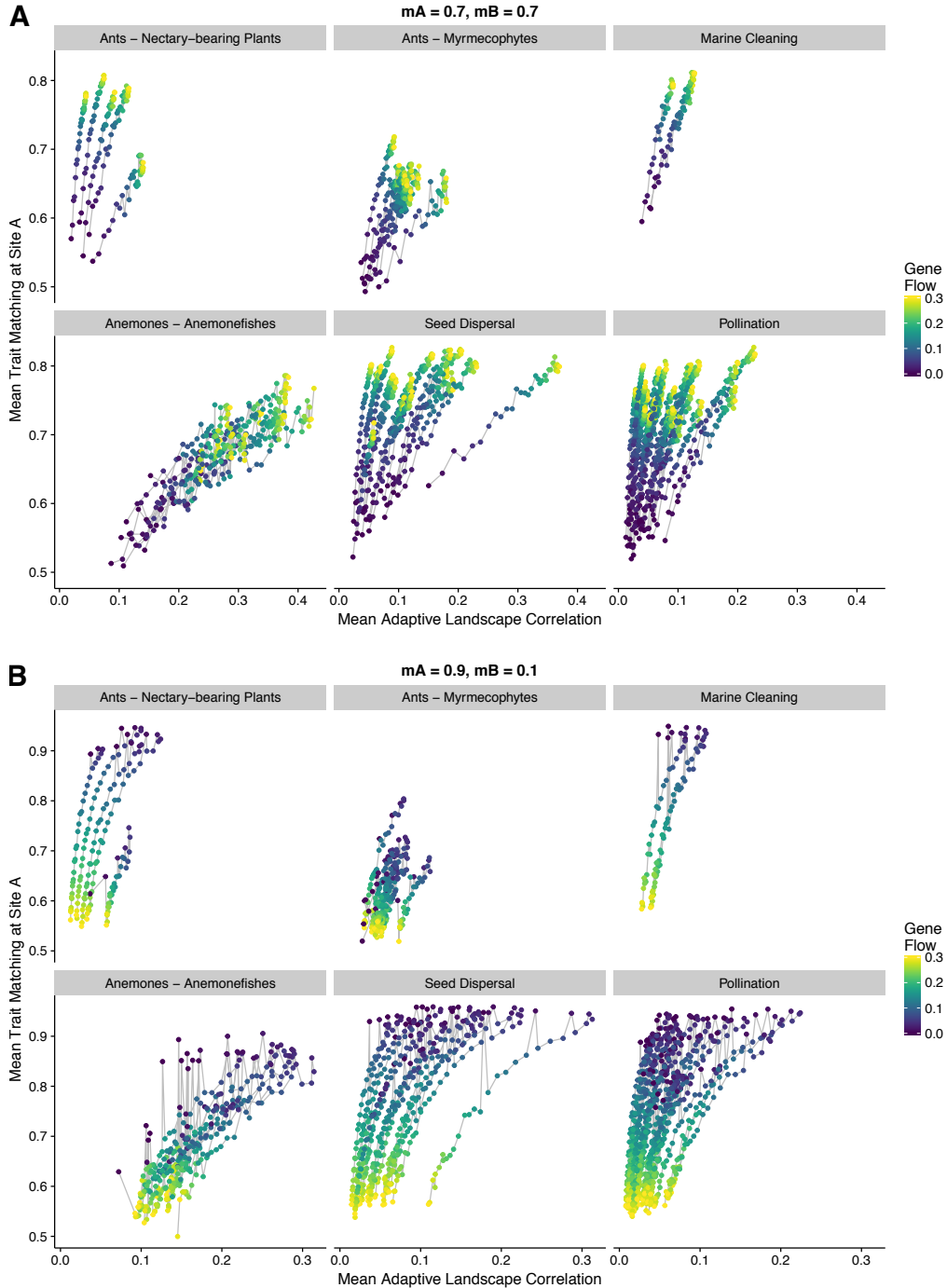


Figure S11: Greater similarity of adaptive landscapes (i.e., greater correlation among rows of matrix  $\mathbf{T}$ ) lead to higher values of trait matching. Each panel shows the mean trait matching at equilibrium at site  $A$  ( $\bar{\tau}_A^*$ ) as a function of the mean correlation among mutualistic adaptive landscapes for different values of gene flow ( $g_i$ , warmer colors depict higher  $g_i$  values) and for the indicated mutualism type. Trait matching and correlation among adaptive landscapes were calculated using our analytical equilibrium expression (eq. [S24]) and simulation results for the two-site coevolutionary model (see *Matrix  $\mathbf{T}$  and the emergence of trait matching*). Each point corresponds to the mean value of 100 simulations and lines connect points from the same empirical mutualistic network ( $n = 72$  networks). (A) Results for two hotspots ( $m_{i,A} = m_{i,B} = 0.7$ ). (B) Results for a hotspot and a coldspot ( $m_{i,A} = 0.9, m_{i,B} = 0.1$ ). Simulation parameters as in Fig. S2.

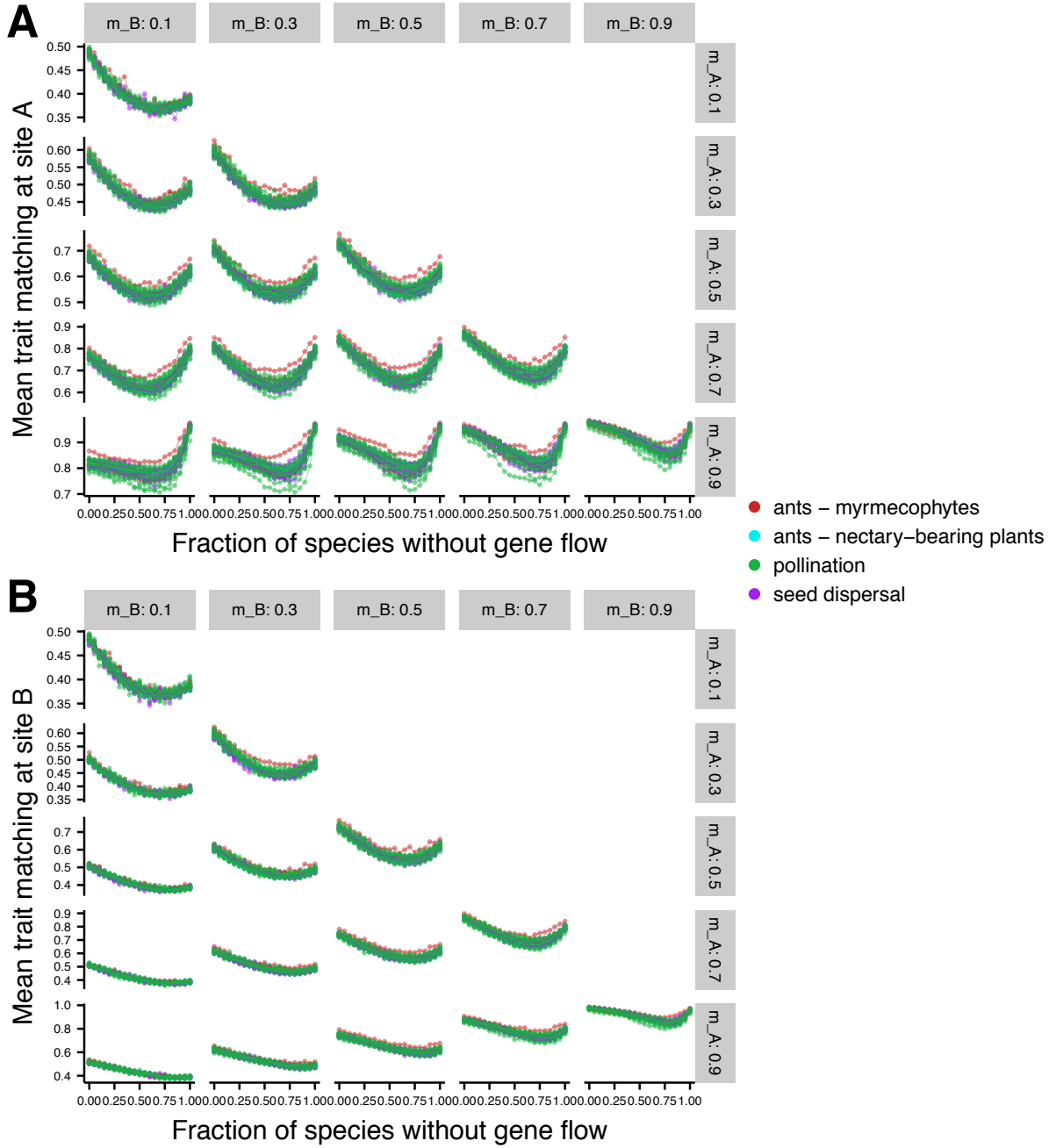


Figure S12: The ongoing disruption of gene flow causes trait matching to decrease in mutualistic networks, but extreme loss of gene flow may lead to a small increase in trait matching. Each panel shows the mean trait matching at equilibrium ( $\bar{\tau}^*$ ) as gene flow is progressively lost in simulations with the indicated values of mutualistic selection ( $m_{i,A}$ : rows,  $m_{i,B}$ : columns). In these simulations, all species in the network start with a high value of gene flow ( $g_i = 0.3 \forall i$ ) and species randomly lose gene flow until all species lack gene flow ( $g_i = 0 \forall i$ ). Trait matching was calculated using our analytical equilibrium expression (eq. [S24]) and empirical data on ecological dependencies for 29 networks in our dataset (Table S1). (A and B) Each point is the mean trait matching for 10 different  $\theta$  samples in each of 10 distinct simulations. Lines connect points from the same network and different colors indicate different types of mutualism. (A) Trait matching at site A. (B) Trait matching at site B. Sample distributions and values for simulation parameters:  $\varphi_{i,A} = \varphi_{i,B} = 1$ ,  $\theta_{i,A} \sim \mathcal{U}[0, 10]$ ,  $\theta_{i,B} \sim \mathcal{U}[10, 20]$ ,  $\alpha = 0.2$ .

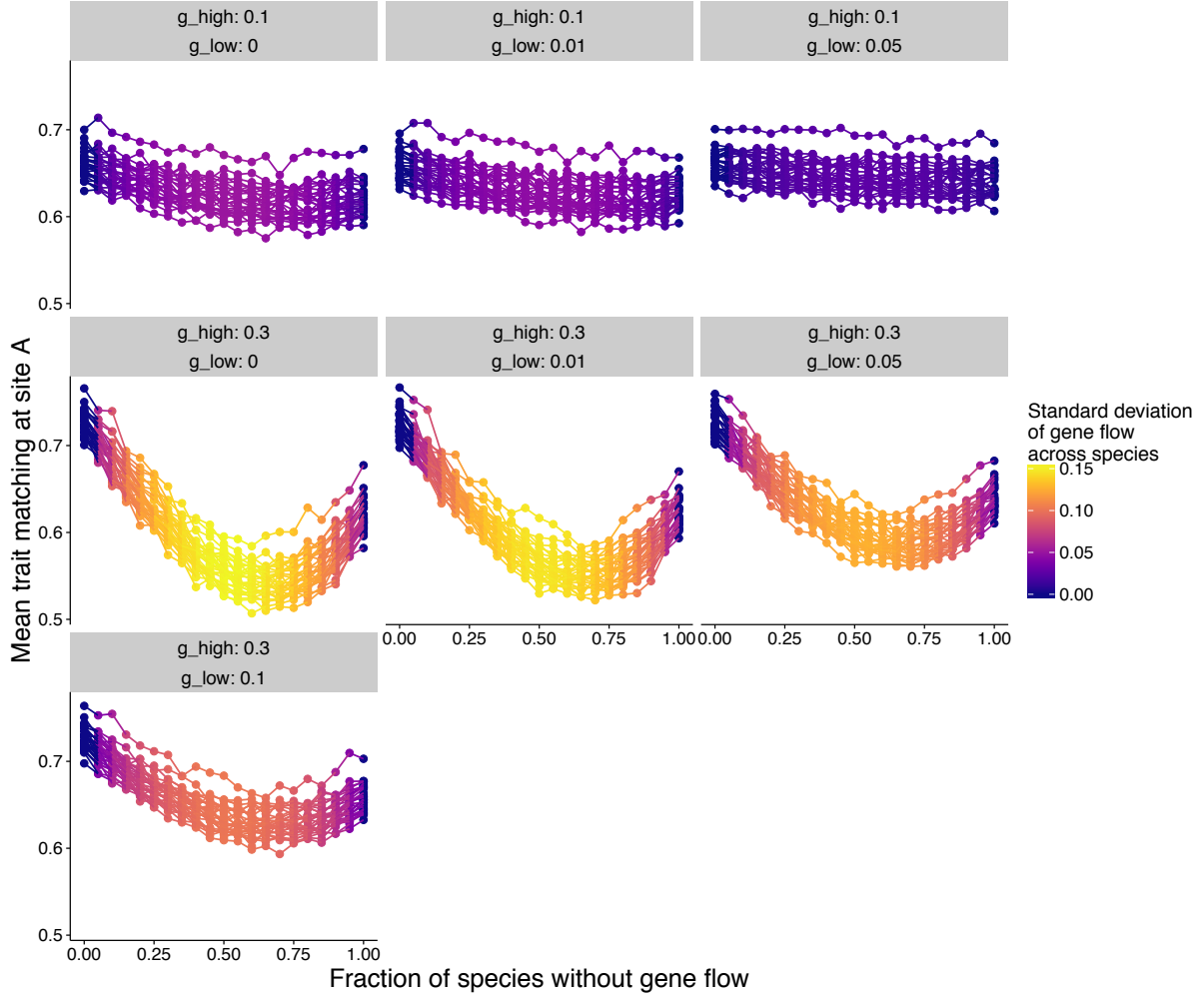


Figure S13: Trait matching in mutualistic networks is affected by the progressive loss of gene flow and the lowest values of trait matching occur when gene flow is highly variable across species in the network. Each panel shows the mean trait matching at equilibrium at site  $A$  ( $\bar{\tau}_A^*$ ) as gene flow is progressively lost in simulations with the indicated parameterization for the high (initial) and low (final) values of gene flow. In these simulations, all species in the network start with a high value of gene flow and species randomly lose gene flow until all species have a low value of gene flow. Trait matching was calculated using our analytical equilibrium expression (eq. [S24]) and empirical data on ecological dependencies for 29 networks in our dataset (Table S1). Each point is the mean trait matching for 10 different  $\theta$  samples in each of 10 distinct simulations and lines connect points from the same network. Warmer colors indicate higher standard deviation in gene flow values across species in the network. Sample distributions and values for simulation parameters:  $\varphi_{i,A} = \varphi_{i,B} = 1$ ,  $\theta_{i,A} \sim \mathcal{U}[0, 10]$ ,  $\theta_{i,B} \sim \mathcal{U}[10, 20]$ ,  $m_{i,A} = m_{i,B} = 0.5$ , and  $\alpha = 0.2$ .

Table S1: Empirical mutualistic networks used in this study. Mutualism: AA, anemones–anemonefishes; AM, ants–myrmecophytes; AN, ants–nectary-bearing plants; MC, marine cleaning; P, pollination; SD, seed dispersal. Each mutualism is identified by two sets of species that interact.  $N_1$ : number of species in the first set (e.g., plant species in the plant-animal mutualisms).  $N_2$ : number of species in the second set.  $N$ : total species richness ( $N = N_1 + N_2$ ).  $C$ : connectance.  $NODF$ : nestedness.  $Q$ : modularity.  $PC1$ : first principal component of a PCA with network metrics.  $PC2$ : second principal component. Availability: IWDB, dataset available for download at [www.nceas.ucsb.edu/interactionweb](http://www.nceas.ucsb.edu/interactionweb); Web of Life, dataset available for download at [www.web-of-life.es](http://www.web-of-life.es); Rico-Gray, dataset kindly provided by Victor Rico-Gray; Izzo, dataset kindly provided by Thiago Izzo; Sazima, dataset kindly provided by Cristina and Ivan Sazima; Donatti, dataset kindly provided by Camila Donatti. \*Network contains quantitative information on the ecological dependencies between species pairs. †Network used in sensitivity analyses.

| Network | Mutualism | $N_1$ | $N_2$ | $N$ | $C$  | $NODF$ | $Q$  | $PC1$ | $PC2$ | Availability      |
|---------|-----------|-------|-------|-----|------|--------|------|-------|-------|-------------------|
| 1†      | AA        | 6     | 5     | 11  | 0.33 | 38.00  | 0.44 | 0.78  | -0.94 | IWDB, (30)        |
| 2†      | AA        | 4     | 5     | 9   | 0.40 | 34.38  | 0.44 | 0.96  | -1.19 | IWDB, (30)        |
| 3       | AA        | 3     | 4     | 7   | 0.50 | 22.22  | 0.33 | 1.41  | -1.39 | IWDB, (30)        |
| 4†      | AA        | 4     | 4     | 8   | 0.44 | 37.50  | 0.37 | 1.47  | -1.09 | IWDB, (30)        |
| 5       | AA        | 5     | 3     | 8   | 0.47 | 38.46  | 0.41 | 1.46  | -1.26 | IWDB, (30)        |
| 6†      | AA        | 4     | 4     | 8   | 0.44 | 62.50  | 0.39 | 2.11  | -0.81 | IWDB, (30)        |
| 7†      | AA        | 4     | 5     | 9   | 0.30 | 12.50  | 0.56 | -0.50 | -1.52 | IWDB, (30)        |
| 8       | AA        | 4     | 4     | 8   | 0.44 | 29.17  | 0.39 | 1.15  | -1.25 | IWDB, (30)        |
| 9       | AA        | 4     | 4     | 8   | 0.38 | 16.67  | 0.47 | 0.23  | -1.47 | IWDB, (30)        |
| 10†     | AA        | 5     | 5     | 10  | 0.32 | 22.50  | 0.48 | 0.12  | -1.24 | IWDB, (30)        |
| 11      | AA        | 4     | 5     | 9   | 0.35 | 12.50  | 0.47 | 0.02  | -1.43 | IWDB, (30)        |
| 12*     | AM        | 8     | 16    | 24  | 0.15 | 4.28   | 0.78 | -2.23 | -1.50 | Web of Life, (31) |
| 13*     | AM        | 15    | 24    | 39  | 0.12 | 12.80  | 0.67 | -1.78 | -0.76 | Web of Life, (32) |
| 14      | AM        | 5     | 6     | 11  | 0.23 | 8.00   | 0.69 | -1.41 | -1.72 | Izzo, (33)        |
| 15†     | AM        | 7     | 9     | 16  | 0.17 | 7.02   | 0.78 | -2.00 | -1.69 | Izzo, (33)        |
| 16†     | AM        | 8     | 13    | 21  | 0.16 | 11.32  | 0.69 | -1.61 | -1.27 | Izzo, (33)        |
| 17†     | AM        | 7     | 8     | 15  | 0.16 | 0.00   | 0.79 | -2.30 | -1.80 | Izzo, (33)        |
| 18†     | AM        | 9     | 12    | 21  | 0.15 | 4.90   | 0.78 | -2.21 | -1.56 | Izzo, (33)        |
| 19      | AM        | 8     | 10    | 18  | 0.15 | 4.11   | 0.78 | -2.20 | -1.63 | Izzo, (33)        |
| 20*     | AN        | 48    | 41    | 89  | 0.14 | 44.82  | 0.30 | 0.28  | 1.56  | Web of Life, (34) |
| 21†     | AN        | 38    | 10    | 48  | 0.25 | 39.17  | 0.37 | 0.54  | 0.23  | Rico-Gray, (35)   |
| 22†     | AN        | 99    | 28    | 127 | 0.10 | 40.59  | 0.47 | -0.80 | 1.98  | Rico-Gray, (35)   |
| 23      | AN        | 12    | 5     | 17  | 0.22 | 2.63   | 0.75 | -1.85 | -1.76 | Rico-Gray, (35)   |
| 24†     | AN        | 46    | 13    | 59  | 0.21 | 35.55  | 0.46 | -0.11 | 0.28  | Rico-Gray, (35)   |
| 25      | MC        | 32    | 4     | 36  | 0.41 | 46.30  | 0.36 | 1.50  | -0.33 | (36)              |
| 26†     | MC        | 35    | 5     | 40  | 0.42 | 70.73  | 0.26 | 2.56  | 0.33  | Sazima, (37)      |
| 27†     | MC        | 50    | 6     | 56  | 0.35 | 64.47  | 0.30 | 1.87  | 0.63  | (38)              |
| 28†     | P         | 84    | 101   | 185 | 0.04 | 14.46  | 0.52 | -2.31 | 2.82  | Web of Life, (39) |
| 29      | P         | 43    | 64    | 107 | 0.07 | 15.36  | 0.53 | -1.78 | 1.15  | Web of Life, (39) |
| 30      | P         | 36    | 25    | 61  | 0.09 | 19.19  | 0.59 | -1.57 | 0.06  | Web of Life, (39) |
| 31*†    | P         | 12    | 102   | 114 | 0.14 | 30.78  | 0.49 | -0.95 | 1.44  | Web of Life, (40) |
| 32*     | P         | 13    | 13    | 26  | 0.42 | 84.93  | 0.23 | 3.16  | 0.30  | Web of Life, (41) |
| 33*     | P         | 17    | 61    | 78  | 0.14 | 52.27  | 0.40 | 0.20  | 1.21  | Web of Life, (42) |
| 34*†    | P         | 16    | 36    | 52  | 0.15 | 35.66  | 0.43 | -0.23 | 0.36  | Web of Life, (42) |
| 35      | P         | 11    | 38    | 49  | 0.25 | 35.97  | 0.36 | 0.49  | 0.22  | Web of Life, (43) |
| 36†     | P         | 24    | 118   | 142 | 0.09 | 15.39  | 0.50 | -1.81 | 1.89  | Web of Life, (44) |
| 37†     | P         | 29    | 81    | 110 | 0.08 | 25.68  | 0.48 | -1.29 | 1.47  | Web of Life, (45) |
| 38*     | P         | 40    | 85    | 125 | 0.08 | 19.31  | 0.43 | -1.37 | 1.81  | Web of Life, (46) |
| 39*†    | P         | 58    | 100   | 158 | 0.09 | 34.35  | 0.30 | -0.59 | 2.96  | IWDB, (47)        |
| 40      | P         | 21    | 45    | 66  | 0.09 | 18.02  | 0.62 | -1.74 | 0.08  | Web of Life, (48) |
| 41†     | P         | 23    | 72    | 95  | 0.08 | 22.88  | 0.58 | -1.64 | 0.88  | Web of Life, (48) |

| Network | Mutualism | $N_1$ | $N_2$ | $N$ | $C$  | $NODF$ | $Q$  | $PC1$ | $PC2$ | Availability      |
|---------|-----------|-------|-------|-----|------|--------|------|-------|-------|-------------------|
| 42*     | P         | 11    | 18    | 29  | 0.19 | 32.07  | 0.48 | -0.20 | -0.39 | Web of Life, (49) |
| 43*     | P         | 14    | 13    | 27  | 0.29 | 51.87  | 0.34 | 1.26  | -0.06 | IWDB, (50)        |
| 44*     | P         | 10    | 12    | 22  | 0.25 | 35.96  | 0.44 | 0.31  | -0.54 | IWDB, (50)        |
| 45*†    | P         | 9     | 56    | 65  | 0.20 | 35.49  | 0.43 | -0.08 | 0.47  | Web of Life, (51) |
| 46      | P         | 18    | 60    | 78  | 0.11 | 13.94  | 0.56 | -1.61 | 0.37  | Web of Life, (52) |
| 47†     | P         | 28    | 53    | 81  | 0.07 | 11.16  | 0.58 | -1.94 | 0.43  | Web of Life, (53) |
| 48†     | P         | 51    | 25    | 76  | 0.15 | 46.36  | 0.32 | 0.34  | 1.26  | IWDB, (54)        |
| 49      | P         | 7     | 33    | 40  | 0.28 | 56.66  | 0.36 | 1.25  | 0.24  | Web of Life, (55) |
| 50*     | P         | 13    | 34    | 47  | 0.32 | 40.96  | 0.26 | 1.27  | 0.33  | Web of Life, (56) |
| 51*†    | P         | 10    | 29    | 39  | 0.15 | 29.54  | 0.54 | -0.72 | -0.26 | IWDB, (57)        |
| 52*†    | P         | 9     | 33    | 42  | 0.15 | 18.66  | 0.62 | -1.33 | -0.55 | IWDB, (57)        |
| 53*     | P         | 10    | 29    | 39  | 0.14 | 26.31  | 0.58 | -0.96 | -0.39 | IWDB, (57)        |
| 54*†    | P         | 8     | 26    | 34  | 0.17 | 23.28  | 0.54 | -0.77 | -0.50 | IWDB, (57)        |
| 55*     | P         | 8     | 27    | 35  | 0.22 | 30.31  | 0.50 | -0.24 | -0.40 | IWDB, (57)        |
| 56*†    | SD        | 7     | 21    | 28  | 0.34 | 50.98  | 0.32 | 1.51  | -0.15 | Web of Life, (58) |
| 57*†    | SD        | 31    | 9     | 40  | 0.43 | 67.66  | 0.22 | 2.64  | 0.35  | Web of Life, (59) |
| 58*†    | SD        | 25    | 16    | 41  | 0.17 | 44.70  | 0.40 | 0.31  | 0.28  | Web of Life, (60) |
| 59*     | SD        | 34    | 20    | 54  | 0.14 | 43.38  | 0.40 | 0.07  | 0.60  | Web of Life, (60) |
| 60*     | SD        | 25    | 13    | 38  | 0.15 | 29.69  | 0.54 | -0.69 | -0.28 | Web of Life, (60) |
| 61*†    | SD        | 21    | 15    | 36  | 0.16 | 34.17  | 0.47 | -0.26 | -0.11 | Web of Life, (60) |
| 62      | SD        | 72    | 7     | 79  | 0.28 | 51.67  | 0.33 | 0.99  | 1.02  | Web of Life, (61) |
| 63      | SD        | 45    | 46    | 91  | 0.13 | 27.80  | 0.41 | -0.67 | 1.13  | Donatti, (62)     |
| 64*†    | SD        | 35    | 29    | 64  | 0.14 | 35.49  | 0.38 | -0.13 | 0.74  | Web of Life, (63) |
| 65†     | SD        | 16    | 17    | 33  | 0.44 | 78.76  | 0.24 | 3.02  | 0.28  | Web of Life, (64) |
| 66      | SD        | 5     | 27    | 32  | 0.64 | 67.34  | 0.18 | 3.67  | -0.25 | Web of Life, (65) |
| 67      | SD        | 24    | 61    | 85  | 0.34 | 58.84  | 0.20 | 1.87  | 1.41  | Web of Life, (66) |
| 68†     | SD        | 29    | 32    | 61  | 0.07 | 11.21  | 0.65 | -2.07 | -0.13 | Web of Life, (67) |
| 69*     | SD        | 4     | 19    | 23  | 0.43 | 48.29  | 0.35 | 1.73  | -0.60 | Web of Life, (68) |
| 70*     | SD        | 13    | 11    | 24  | 0.37 | 73.90  | 0.25 | 2.56  | 0.17  | Web of Life, (68) |
| 71*     | SD        | 33    | 88    | 121 | 0.14 | 34.58  | 0.31 | -0.20 | 2.06  | Web of Life, (69) |
| 72†     | SD        | 7     | 6     | 13  | 0.52 | 66.67  | 0.26 | 3.02  | -0.55 | Web of Life, (70) |

Table S2: List of parameters and variables used in the numerical simulations of the two-site coevolutionary model. Parameter/variable: mathematical notation for each parameter/variable (site  $S$  is either  $A$  or  $B$ ). Definition: verbal definition of parameters/variables. Sampling distribution: statistical distribution used to sample parameters/variables for each species. Values for simulations: values used to sample parameters/variables or the values attributed to parameters/variables in simulations (values in **bold** indicate the main set of simulations reported in the main text).

| Parameter/<br>variable | Definition   | Sampling distribution  | Values for simulations   |
|------------------------|--|--|--|
| $m_{i,S}$              | Level of mutualistic selection of species $i$ at site $S$  | $\mathcal{N}[\mu = \bar{m}_S, \sigma^2 = 0.0001]; 0 \leq m_{i,S} \leq 1$                         | $(\bar{m}_A, \bar{m}_B) = (0.1, 0.1); (0.3, 0.1); (0.5, 0.1); (0.7, 0.1); (\mathbf{0.9}, \mathbf{0.1}); (0.3, 0.3); (0.5, 0.3); (0.7, 0.3); (0.9, 0.3); (0.5, 0.5); (0.7, 0.5); (0.9, 0.5); (\mathbf{0.7}, \mathbf{0.7}); (0.9, 0.7); (0.9, 0.9)$            |
| $g_i$                  | Level of gene flow of species $i$ across sites   | $\mathcal{N}[\mu = \bar{g}, \sigma^2 = \mathbf{0.000001} \text{ or } 0.0001]; 0 \leq g_i \leq 1$ | $\bar{g} = \mathbf{0}; \mathbf{0.01}; \mathbf{0.02}; \dots; \mathbf{0.29}; \mathbf{0.3}$   |
| $\theta_{i,S}$         | Trait value of species $i$ selected by the environment at site $S$   | $\mathcal{U}[\theta_{S,min}, \theta_{S,max}]; \theta_{i,S} > 0$                                  | $([\theta_{A,min}, \theta_{A,max}], [\theta_{B,min}, \theta_{B,max}]) = ([0, 10], [0, 10]); ([0, 10], [5, 15]); ([\mathbf{0}, \mathbf{10}], [\mathbf{10}, \mathbf{20}]); ([0, 10], [20, 30]); ([0, 10], \theta_{i,A} + \mathcal{N}(\mu = 10, \sigma^2 = 1))$ |
| $\varphi_{i,S}$        | Additive genetic variance of trait $z_{i,S}$ multiplied by the slope of the selection gradient ( $\varphi_{i,S} = \sigma_{G_{z_{i,S}}}^2 \rho_{i,S}$ ) | $\mathcal{N}[\mu = \bar{\varphi}_S, \sigma^2 = 0.0001]; \varphi_{i,S} > 0$                       | $\bar{\varphi}_S = 0.1; \mathbf{0.5}; 1$   |
| $\alpha$               | Sensitivity of trait matching to differences between traits  | -  | $\alpha = 0.05; \mathbf{0.2}; 0.8$ (same value for all species; $\alpha > 0$ )   |
| $N_S$                  | Number of species in the mutualistic assemblage at site $S$  | -  | Parameterized with empirical networks (see Table S1)   |
| $\mathbf{A} (a_{ij})$  | Adjacency matrix describing if species $i$ and $j$ interact ( $a_{ij} = 1$ ) or not ( $a_{ij} = 0$ ) in a mutualistic assemblage                       | -  | Parameterized with empirical networks (see Table S1)   |
| $z_{i,S}^{(t)}$        | Mean trait value of the population of species $i$ at site $S$  | Sampled at $t = 0$ from $\mathcal{U}[\theta_{S,min}, \theta_{S,max}]; z_{i,S}^{(t)} > 0$         | Values change over time according to equation [S7]   |
| $\tau_{ij,S}^{(t)}$    | Trait matching between species $i$ and $j$ at site $S$   | -  | Values change over time according to $z_{i,S}^{(t)}$ and $z_{j,S}^{(t)}$ (eq. [S5]; $0 \leq \tau_{ij,S}^{(t)} \leq 1$ )  |
| $q_{ij,S}^{(t)}$       | Evolutionary effect of species $j$ on species $i$ at site $S$  | -  | Values change over time according to $\tau_{ij,S}^{(t)}$ (eq. [S6]; $0 \leq q_{ij,S}^{(t)} \leq 1; \sum_{j=1}^{N_S} q_{ij,S}^{(t)} = m_{i,S}$ )  |

Table S3: Correlations between the first principal components ( $PC1$  and  $PC2$ ) and our four metrics of network structure.

|                       | $PC1$ | $PC2$ |
|-----------------------|-------|-------|
| richness ( $N$ )      | -0.22 | 0.81  |
| connectance ( $C$ )   | 0.56  | -0.35 |
| nestedness ( $NODF$ ) | 0.58  | 0.27  |
| modularity ( $Q$ )    | -0.56 | -0.39 |